Mathematical modeling of N-803 treatment in SIV-infected non-human primates

Jonathan W. Cody[1], Amy L. Ellis-Connell[2], Shelby L. O'Connor[2], Elsje Pienaar[1*]

[1] Weldon School of Biomedical Engineering, Purdue University, West Lafayette, Indiana, United States of America

[2] Department of Pathology and Laboratory Medicine, University of Wisconsin-Madison, Madison, Wisconsin, United States of America

* Corresponding author

E-mail: epienaar@purdue.edu

Abstract

Immunomodulatory drugs could contribute to a functional cure for Human Immunodeficiency Virus (HIV). Interleukin-15 (IL-15) promotes expansion and activation of $CD8^+$ T cell and natural killer (NK) cell populations. In one study, an IL-15 superagonist, N-803, suppressed Simian Immunodeficiency Virus (SIV) in non-human primates (NHPs) who had received prior SIV vaccination. However, viral suppression attenuated with continued N-803 treatment, partially returning after long treatment interruption. While there is evidence of concurrent drug tolerance, immune regulation, and viral escape, the relative contributions of these mechanisms to the observed viral dynamics have not been quantified. Here, we utilize mathematical models of N-803 treatment in SIV-infected macaques to estimate contributions of these three key mechanisms to treatment outcomes: 1) drug tolerance, 2) immune regulation, and 3) viral escape. We calibrated our model to viral and lymphocyte responses from the above-mentioned NHP study. Our models track $CD8^+$ T cell and NK cell populations with N-803-dependent proliferation and activation, as well as viral dynamics in response to these immune cell populations. We compared mathematical models with different combinations of the three key mechanisms based on Akaike Information Criterion and important qualitative features of the NHP data. Two minimal models were capable of reproducing the observed SIV response to N-803. In both models, immune regulation strongly reduced cytotoxic cell activation to enable viral rebound. Either long-term drug tolerance or viral escape (or some combination thereof) could account for changes to viral dynamics across long breaks in N-803 treatment. Theoretical explorations with the models showed that less-frequent N-803 dosing and concurrent immune regulation blockade (e.g. PD-L1 inhibition) may improve N-803 efficacy. However, N-803 may need to be combined with other immune therapies to countermand viral escape from the $CD8^+$ T cell response. Our mechanistic model will inform such therapy design and guide future studies.

Author summary

Immune therapy may be a critical component in the functional cure for Human Immunodeficiency Virus (HIV). N-803 is an immunotherapeutic drug that activates antigen-specific $CD8^+$ T cells of the immune system. These $CD8^+$ T cells eliminate HIV-infected cells in order to limit the spread of infection in the body. In one study, N-803 reduced plasma viremia in macaques that were infected with Simian Immunodeficiency Virus, an analog of HIV. Here, we used mathematical models to analyze the data from this study to better understand the effects of N-803 therapy on the immune system. Our models indicated that inhibitory signals may be reversing the stimulatory

effect of N-803. Results also suggested the possibilities that tolerance to N-803 could build up within the $CD8^+$ T cells themselves and that the treatment may be selecting for virus strains that are not targeted by $CD8^+$ T cells. Our models predict that N-803 therapy may be made more effective if the time between doses is increased or if inhibitory signals are blocked by an additional drug. Also, N-803 may need to be combined with other immune therapies to target virus that would otherwise evade $CD8^+$ T cells.

Introduction

In 2019, there was an estimated 38.0 million people living with Human Immunodeficiency Virus (HIV) and 690,000 deaths related to Acquired Immune Deficiency Syndrome (AIDS) [1]. Current antiretroviral therapy (ART) remains a life-long therapy, since treatment interruption inevitably leads to viral rebound [2]. Alternative treatment strategies include reversing latent infections [3], introducing cellular and humoral vaccines [4], enhancing T cell function [5], and enhancing NK cell function [6]. These immune-based approaches could reduce the reliance on continuous and lifelong ART and contribute to a functional HIV cure.

One immunotherapeutic approach involves interleukin-15 (IL-15). Interleukin-15 is a cytokine that induces proliferation and activation of $CD8^+$ T cells and natural killer (NK) cells (reviewed in [7, 8]). Although treatment with monomeric IL-15 did not lower plasma viral load in non-human primates (NHPs) infected with Simian Immunodeficiency Virus (SIV) [9, 10], treatment with the heterodimeric IL-15/IL-15Rα complex did reduce viral load in plasma and lymph tissue of NHPs infected with Simian/Human Immunodeficiency Virus (SHIV) [11]. N-803 [ImmunityBio] (formerly ALT-803 [Altor Biosciences]) is an IL-15 superagonist that combines an IL-15 variant with improved bioactivity [12] with an IL-15Rα-Fc complex to extend serum half-life and bioavailability [13]. This superagonist induced proliferation of $CD8^+$ T cells and NK cells in healthy NHPs [14, 15], SIV-infected NHPs [15, 16], and in humans participating in cancer trials [17-19]. In one NHP study, N-803 treatment reduced the number of SIV-infected cells in B-cell follicles but did not consistently lower plasma viral load [15]. In a different cohort of NHPs genetically predisposed to SIV control and vaccinated prior to infection, weekly doses of N-803 successfully lowered SIV viral load in the plasma, though the effect was transient [16]. After initially being suppressed, the viral load partially rebounded during the first month of weekly doses. However, after a 29 week break in treatment, N-803 regained partial efficacy in reducing plasma viral load. Thus, there were variations in treatment efficacy along both short (weeks) and long (months) timescales. While this is only one study, these dynamic responses provide a unique opportunity to quantify transient

treatment responses and suggest that changes in treatment scheduling of N-803 could improve efficacy in reducing SIV viral load. However, such optimization would require an understanding of the underlying mechanisms driving the observed loss and recovery of treatment efficacy.

The vaccinated NHP study identified several mechanisms which could have compromised the efficacy of N-803 [16]. We broadly consider these mechanisms in three categories (Table 1). The first mechanism, drug tolerance, was evidenced by the decline of IL-15 receptor expression by $CD8^+$ T cells and NK cells during N-803 treatment, thereby reducing the available targets for N-803. The second mechanism we term immune regulation. Expression of inhibitory markers (CD39 and PD-1) by $CD8^+$ T cells and NK cells increased, as did the presence of regulatory T cells ($CD4^+CD25^+CD39^+$ phenotype) in the peripheral blood. In other studies, N-803 increased serum levels of the anti-inflammatory cytokine IL-10 in mice [20], and, in a mouse model of cerebral malaria, N-803 induced NK cells to secrete IL-10, which decreased $CD8^+$ T cell activation in the brain [21]. Together, these data indicate that there may be a systemic anti-inflammatory response that could hamper the ability of N-803 to stimulate prolonged anti-viral immune responses. In this work we broadly group these anti-inflammatory responses under the term immune regulation. Third, the amino acid sequence of targeted $CD8^+$ T cell epitopes was altered during N-803 treatment, which could be consistent with viral escape [16]. As a result, previously generated $CD8^+$ T cells may not recognize circulating viral variants [22-24]. While evidence of all three of these mechanisms exists in the NHP data, the contributions of each mechanism to the loss and recovery of viral suppression under N-803 therapy have not been quantitatively assessed, a task that is difficult to do experimentally.

Table 1. Mechanisms considered to compromise N-803 efficacy.

Drug Tolerance	Factors which act only to diminish the stimulatory effect of N-803 on $CD8^+$ T cells and NK cells (e.g. downregulation of IL-15 receptors)
Immune Regulation	Factors which act to inhibit the immune response of CD8+ T cells and NK cells (e.g. upregulation of immune checkpoint molecules)
Viral Escape	Selection of SIV variants that evade the $CD8^+$ T cell immune response

Computational models are well-suited to quantify and deconvolute the effects of multiple interacting mechanisms in complex systems. Ordinary differential equation (ODE) models have been used to study HIV and its treatment (reviewed in [25, 26]). ODE models have investigated the potential of various treatment strategies, including reactivating latent infections [27, 28],

cytotoxic cell stimulation [27], and cellular vaccines [29]. Modelers have also explored how immune regulation [30, 31] and viral escape [29, 32] affect cytotoxic cell function and HIV infection.

Here we combine, for the first time, pharmacokinetics and pharmacodynamics of N-803 with an HIV infection model that includes both cytotoxic T-cell and NK cell populations. We also newly combine this model with mechanisms which may lower N-803 efficacy. These mechanisms are: drug tolerance that weakens the N-803 effect in cytotoxic cells; immune regulatory signals that inhibit cytotoxic cell function; and viral escape from cytotoxic cell targeting. We calibrated the model to data from one vaccinated NHP study, specifically to longitudinal viral, $CD8^+$ T cell, and NK cell measurements from the peripheral blood [16]. We applied the model to quantify how drug tolerance, immune regulation, and viral escape may have contributed to the dynamics of SIV viremia during N-803 treatment in this unique set of NHPs. We also predicted how these mechanisms might impact potential improvements to N-803 regimens.

Methods

Mathematical model

Viral infection. We followed the practice of representing the within-host dynamics of viral infection with a system of ordinary differential equations [25-32]. Equations (1-4) describe the model of viral infection and immune response in the absence of N-803 treatment. This is a single-compartment model that does not explicitly consider migration between blood, lymph, and peripheral tissues. The disease model is graphically summarized in Fig 1A. Table 2 lists the dependent variables of the model.

Table 2. Model variables.

	Variable	Symbol	Units
Infection model	Cell infected with SIV variant V	$[I_V]$	#/μL
	Cell infected with SIV escape variant W	$[I_W]$	#/μL
	$CD8^+$ T cells in peripheral blood	$[E]$	#/μL
	Natural killer cells in peripheral blood	$[K]$	#/μL
Treatment model	N-803 at absorption site	$[X]$	pmol/kg
	N-803 in plasma	$[C]$	pM
	Tolerance variables	$[\mathrm{TOL}_1]\ldots[\mathrm{TOL}_N]$	-
	Regulation variables	$[\mathrm{REG}_1]\ldots[\mathrm{REG}_M]$	-

Dependent variables from Eq. (1-14) and Fig 1, shown with their corresponding symbol and units.

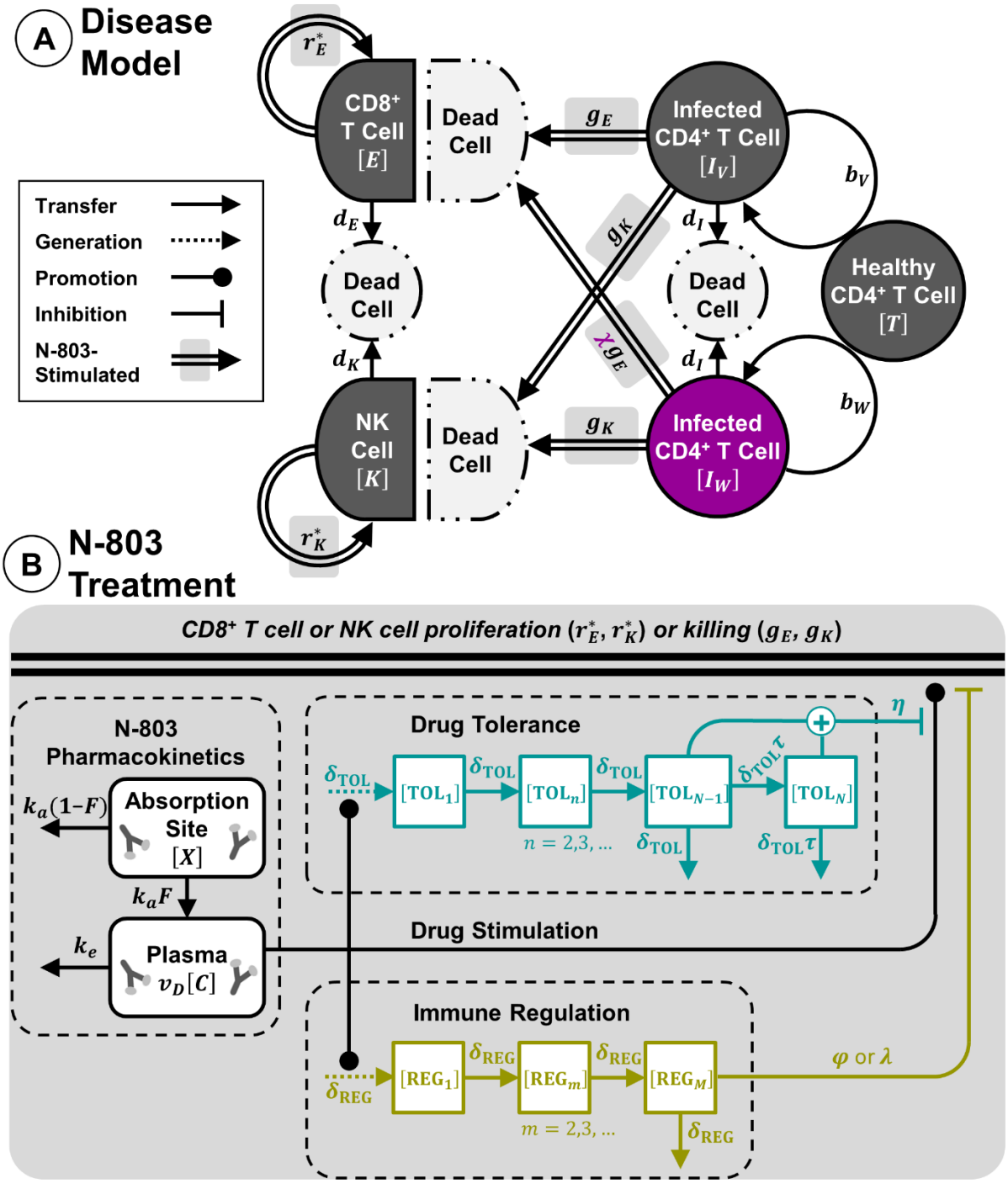

Fig 1. Mathematical model of N-803 treatment of SIV. (A) SIV disease model includes cells infected with one of two variants of SIV virus (I_V and I_W), along with CD8⁺ T cells (E) and NK cells (K) (Eq. 1-4). Proliferation rate constants r^*_E and r^*_K for CD8⁺ T cells and NK cells are modified by density-dependent terms (not shown, see Eq. 3,4). (B) N-803 treatment model includes pharmacokinetics at absorption site and plasma compartments (Eq. 5,6). N-803 stimulates proliferation and cytotoxicity of CD8⁺ T cells and NK cells, where drug effect is inhibited by tolerance (Eq. 7-12). Immune regulation inhibits proliferation and cytotoxicity of cells (Eq. 7,8,13,14). Double lines indicate the sum of drug-induced and constitutive rates.

Healthy CD4$^+$ T cells are assumed to be constant, and free virions are assumed to be proportional to infected cells (assumptions are discussed in S1 Appendix). The latter assumption is common in HIV models [29, 32-34] and reduces model complexity while still allowing calibration to experimentally measured fold changes in viral load. In Eq. (1), infected cells, I_V, infect healthy CD4$^+$ T cells, T, with rate constant b_V. This infection represents both cell-free and cell-to-cell transmission. Infected cells, I_V, die with rate constant d_I (Eq. 1). CD8$^+$ T cells, E, and NK cells, K, kill infected cells with second-order rate constants g_E and g_K, respectively (Eq. 1). For simplicity, these constants (g_E and g_K) are applied to the total populations of CD8$^+$ T cells and NK cells (see S1 Appendix). Changes in the frequency of cytotoxically active cells within these two groups are represented by modifications to these average killing rates (see next subsection, 'N-803 treatment').

Viral escape from the CD8$^+$ T cell response is a phenomena documented in both HIV and SIV [22-24]. Our data subjects included two animals with the *Mamu-B*08* MHC class I allele which had received vaccination with *Mamu-B*08* restricted viral epitopes [35]. Sequencing revealed changes in the amino acid composition of *Mamu-B*08* restricted epitopes after N-803 treatment, changes which could have occurred during viral escape [16]. Viral escape was incorporated into the model by including two viral variants and no mutation between the variants, following Asquith et. al. [36, 37]. The cells infected with the escape variant, I_W (Eq. 2), have reduced susceptibility to cytotoxic T cells (by applying a factor χ<1 to the killing rate). This variant also infects target cells at a lower rate constant (b_W<b_V), as escape can often incur a fitness penalty [38-40].

Both T cells [41, 42] and NK cells [43] are maintained by self-renewal. In our model, CD8$^+$ T cells and NK cells proliferate with rate constants r_E and r_K and undergo apoptosis with rate constants d_E and d_K, respectively (Eq. 3,4). To maintain a stable population, proliferation and survival are thought to be density-dependent, which could arise from competition for space and cytokines [44]. Therefore, our proliferation rates are modified by density-dependent terms governed by h (Eq. 3,4) [27, 45].

$$[I_V]' = b_V T[V] - d_I[I_V] - g_E[E][I_V] - g_K[K][I_V] \quad (1)$$

$$[I_W]' = b_W T[W] - d_I[I_W] - \chi g_E[E][I_W] - g_K[K][I_W] \quad (2)$$

$$[E]' = r_E\left(\frac{h}{h+[E]}\right)[E] - d_E[E] \quad (3)$$

$$[K]' = r_K\left(\frac{h}{h+[K]}\right)[K] - d_K[K] \tag{4}$$

N-803 treatment. The pharmacokinetics for N-803 (Fig 1B) follows the basic model for extravascular dosing [46]. The quantity of N-803 at the absorption site, X, and concentration of N-803 in the plasma, C, are described by Eq. (5,6). Parameters k_a, k_e, F, and v_d are the absorption rate constant, elimination rate constant, bioavailability, and volume of distribution, respectively.

N-803 has been demonstrated to expand CD8$^+$ T cells and NK cells in healthy NHPs [14, 15], SIV-infected NHPs [15, 16], and in humans participating in cancer trials [17-19]. N-803 also increased expression of cytolytic proteins perforin and granzyme B in human CD8$^+$ T cells [14] and NK cells in vitro [47, 48] and induced secretion of cytokines IFNγ and TNFα in murine CD8$^+$ T cells and NK cells in vivo [20, 49, 50]. Therefore, we represented N-803 pharmacodynamics by applying a drug-dependent increase (Eq. 7,8, Fig 1B) to both the rates of killing and proliferation for CD8$^+$ T cells and NK cells (parameters g_E,g_K and r_E,r_K in Eq. 1-4). Effects saturate for both cell types according to a single parameter, C_{50} (Eq. 7,8). The parameters γ_E,γ_K and ρ_E,ρ_K ('Drug Effect' in Eq. 7,8) are the maximum relative increases in killing and proliferation rates, respectively. The contribution of drug tolerance and immune regulation (also shown in Eq. 7,8) will be discussed in the following paragraphs.

$$[X]' = -k_a[X] \tag{5}$$

$$[C]' = k_a(F/v_d)[X] - k_e[C] \tag{6}$$

$$g_i \to g_i\left[1+\overbrace{\gamma_i\left(\frac{[C]}{C_{50}+[C]}\right)}^{\text{Drug Effect}}\overbrace{\left(\frac{1}{1+\eta([\mathrm{TOL}_{N-1}]+[\mathrm{TOL}_N])}\right)}^{\text{Drug Tolerance}}\right]\overbrace{\left(\frac{1}{1+\lambda[\mathrm{REG}_M]}\right)}^{\text{Immune Regulation}} \quad i=E,K \tag{7}$$

$$r_i \to r_i\left[1+\rho_i\left(\frac{[C]}{C_{50}+[C]}\right)\left(\frac{1}{1+\eta([\mathrm{TOL}_{N-1}]+[\mathrm{TOL}_N])}\right)\right]\left(\frac{1}{1+\varphi[\mathrm{REG}_M]}\right) \quad i=E,K \tag{8}$$

In the N-803 treated NHPs, expression of the IL-15 receptor subunits, CD122 and CD132, declined in both CD8$^+$ T cells and NK cells with continued treatment, suggesting a possible tolerance to N-803 [16]. Furthermore, the proliferation of CD8$^+$ T cells and NK cells was weaker in the second and third treatment cycles compared to the first cycle [16]. We phenomenologically

represented drug tolerance by adding a delayed inhibition to the drug effect ('Drug Tolerance' term in Eq. 7,8), the strength of which is governed by the parameter η. The onset of tolerance is delayed from the drug effect term $[C]/(C_{50}+[C])$ according to the parameters δ_{TOL} and τ (Eq. 9-12). The additional parameter τ allows a portion of the drug tolerance to persist long-term and attenuate N-803 stimulation in the third cycle.

$$\left[\mathrm{TOL}_1\right]' = \delta_{\mathrm{TOL}}\left(\frac{[C]}{C_{50}+[C]} - \left[\mathrm{TOL}_1\right]\right) \tag{9}$$

$$\left[\mathrm{TOL}_n\right]' = \delta_{\mathrm{TOL}}\left(\left[\mathrm{TOL}_{n-1}\right] - \left[\mathrm{TOL}_n\right]\right) \quad n = 2,3,\ldots N-2 \tag{10}$$

$$\left[\mathrm{TOL}_{N-1}\right]' = \delta_{\mathrm{TOL}}\left(\left[\mathrm{TOL}_{N-2}\right] - (1+\tau)\left[\mathrm{TOL}_{N-1}\right]\right) \tag{11}$$

$$\left[\mathrm{TOL}_N\right]' = \delta_{\mathrm{TOL}}\left(\tau\left[\mathrm{TOL}_{N-1}\right] - \tau\left[\mathrm{TOL}_N\right]\right) \tag{12}$$

N-803 treatment of NHPs also coincided with increases in regulatory T cell counts ($CD4^+CD25^+CD39^+$ phenotype) in the peripheral blood and increases in expression of inhibitory markers CD39 in $CD8^+$ T cells and PD-1 in NK cells [16]. Other studies found that N-803 increased levels of IL-10 in mice, which decreased cytotoxic T cell activation [20, 21], though IL-10 was not collected along with the NHP data used in our study. Taken together, this implicates a number of regulatory mechanisms that could counteract the immune stimulatory impact of N-803. As with drug tolerance, we employed a single phenomenological representation of the effects of these immune regulatory pathways (i.e. regulatory T cells, IL-10, etc.), rather than mechanistically modeling each specific pathway. Like tolerance, the timing of the regulatory effect was modeled as a delay from the drug effect, this time according to a single parameter δ_{REG} (Eq. 13,14, Fig 1B). Unlike long-term tolerance, incorporating long-term regulation did not improve model fit to data (see S1 Appendix). For the sake of simplicity, it is therefore assumed that the regulatory signals do not persist across the long break in treatment. Immune regulation directly inhibits $CD8^+$ T cell and NK cell killing (both constitutive and drug-induced rates) according to the parameter λ and similarly reduces $CD8^+$ T cell and NK cell proliferation rates according to parameter φ ('Immune regulation' in Eq. (7,8)).

$$\left[\mathrm{REG}_1\right]' = \delta_{\mathrm{REG}}\left(\frac{[C]}{C_{50}+[C]} - \left[\mathrm{REG}_1\right]\right) \tag{13}$$

$$\left[\mathrm{REG}_m\right]' = \delta_{\mathrm{REG}}\left(\left[\mathrm{REG}_{m-1}\right] - \left[\mathrm{REG}_m\right]\right) \quad m = 2,3,\ldots M \tag{14}$$

All of the parameters governing drug tolerance and immune regulation were assumed to be shared between $CD8^+$ T cells and NK cells. This was necessary to improve identifiability of those parameters and simplify analysis.

Experimental data

Our mathematical models were calibrated to a single non-human primate study [16]. Three rhesus macaques, chronically infected with SIVmac239 for at least 1.5 years, were given weekly 0.1 mg/kg subcutaneous doses of N-803. The regimen (Fig 2D) consisted of three cycles of four treatments each, with a 2 week break between the first and second cycles and a 29 week break between the second and third cycles. Assays to measure plasma viremia (quantified as SIVmac239 gag copy equivalents/mL plasma), as well as $CD8^+$ T cells and NK cells in the peripheral blood, were used as calibration data. We assume SIVmac239 gag copy equivalents in the plasma to be proportional to SIV virions in the peripheral blood. Additional quantities were measured in the peripheral blood, which here served to inform the model. These include $CD4^+$ T cells, regulatory T cells ($CD4^+CD25^+CD39^+$ phenotype), CD39 expression in $CD8^+$ T cells, and ki-67, PD-1, CD122, and CD132 expression in $CD8^+$ T cells and NK cells. All animals had been vaccinated with SIV epitopes prior to infection and had previously demonstrated transient SIV control as part of a previous study [35].

Results

Mathematical model reproduced key aspects of observed dynamics of SIV viremia, $CD8^+$ T cells, and NK cells during N-803 treatment.

The full model (Eq. 1-14) was calibrated to SIV in the plasma, and $CD8^+$ T cells and NK cells in the peripheral blood (see S1 Appendix for calibration details). The model reproduced four key characteristics of the SIV plasma viral load during N-803 treatment (Fig 2A). First, the viral load fell sharply during the first 1-2 weeks of treatment (1.10-1.42 log reduction in the model; 1.43-2.08 log reduction in the NHP data) and began to rebound between the first and third week. Second, treatment cycle 2 had a negligible effect as compared to treatment cycle 1. Third, after treatment cycle 2, the viral load settled to a lower set-point (0.58-0.79 log below pre-treatment viral load in the model; 0.38-0.76 log below in the NHP data). Fourth, the viral response to treatment cycle 3 was similar to the response in treatment cycle 1 but less pronounced (0.04-0.53 log reduction in the model; 0.67-1.30 log reduction in the NHP data).

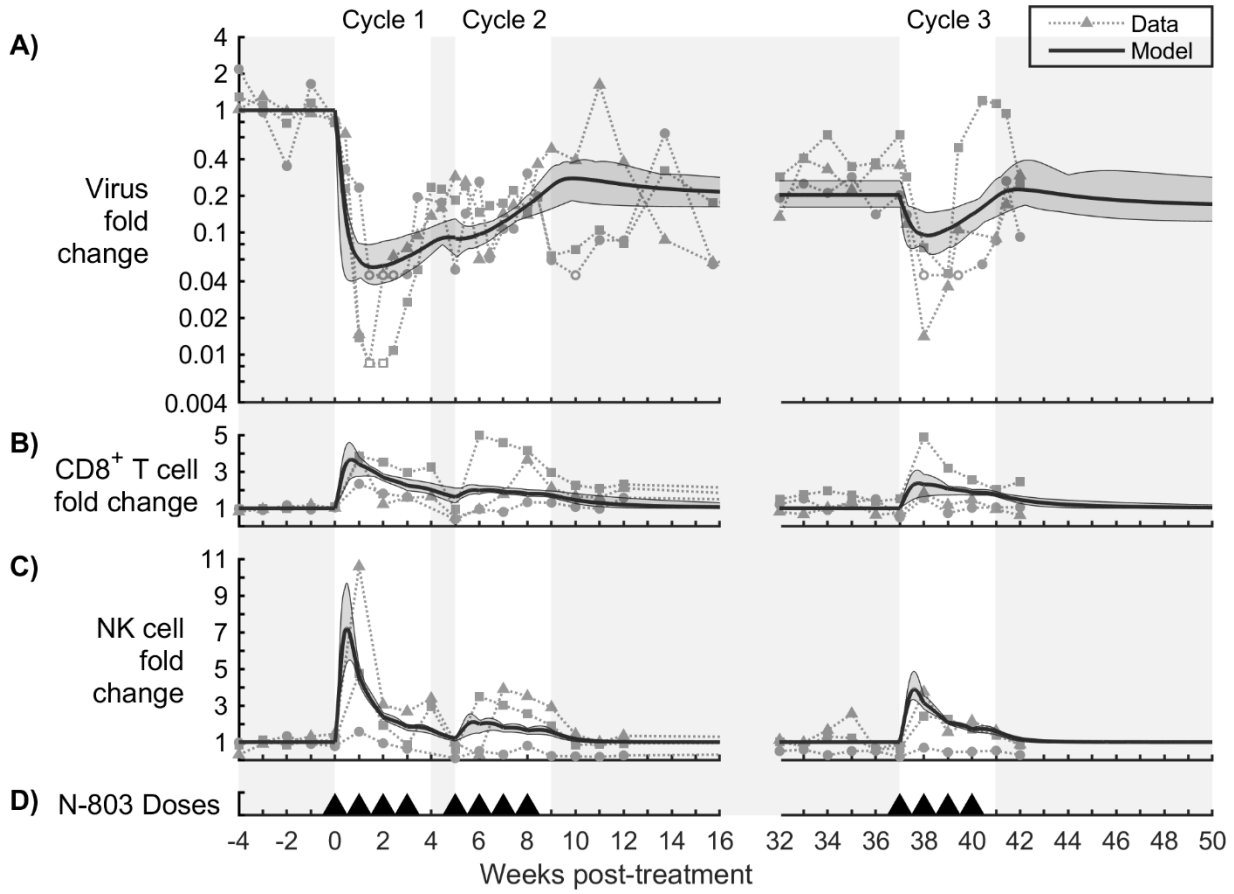

Fig 2. Model calibration to N-803-treated SIV-infected NHP data. The model was calibrated to (A) fold change in virus in the plasma, (B) fold change in $CD8^+$ T cells in the peripheral blood, and (C) fold change in NK cells in the peripheral blood. Panel (D) shows timing of 0.1 mg/kg subcutaneous doses of N-803. Model outputs are shown as the mean (solid line) and range (shaded region) of model outputs from the top 20 parameter sets (lowest NLL) from the calibration procedure. Methodological details and fitted parameter values are given in S1 Appendix. Data from N-803-treated SIV-infected NHPs are shown as different symbols for each NHP [16]. Open symbols represent viral load below the detection limit of the assay (100 viral RNA copies/mL).

The model reproduced two characteristics of the response of peripheral blood $CD8^+$ T cells and NK cells to N-803 (Figs 2B and 2C). First, $CD8^+$ T cells rose quickly in the first week (2.5- to 4.5-fold in the model; 2- to 4-fold in the NHP data), and NK cells expanded even further (5.5- to 9.5-fold in the model; 1.5- to 10.5-fold in the NHP data). Second, both cell populations began to contract in the blood after 1 week of treatment. Although the model attributes this contraction to cell death, it may have also been due to cell migration out of the blood. IL-15 has been shown to promote migration to lymph tissue [15, 51].

Immune regulation, coupled with either drug tolerance or viral escape, can reproduce the viral trajectory

The full model of N-803 treatment of SIV (Fig 1) includes three broad mechanisms that can contribute to reduced N-803 efficacy over time: drug tolerance, immune regulation and viral escape. Drug tolerance represents factors which reduce the cells susceptibility to N-803 long-term (Eq. 7-12), such as the downregulation of surface receptors. Immune regulation represents mechanisms that directly inhibit $CD8^+$ T cell and NK cell proliferation and activation short-term (Eq. 7,8,13,14), which may include increased expression of PD-1 and CD39, increased presence of regulatory T cells, or increased presence of IL-10. Viral escape represents selection of SIV variants that are not recognized by existing $CD8^+$ T cells (Eq. 1,2). The importance of drug tolerance, immune regulation, and viral escape to the dynamics of SIV during N-803 treatment regimen was assessed by systematically removing each mechanism and recalibrating the model, comparing to the full model as a control (Fig 3). Models were compared quantitatively using Negative Log-Likelihood (NLL), a measure of model fit to the data, and Akaike Information Criterion (AIC), which also considers model simplicity (Fig 3A, middle panel). We also compared model performance to qualitative characteristics of the experimental data (Fig 3A, right panel). These qualitative criteria include: drop and rebound of the viral load in cycle 1, negligible viral response in cycle 2, and moderate viral response in cycle 3 (moderate with respect to cycle 1). Additional details on model comparison can be found in S1 Appendix.

Without immune regulation (model #2, Fig 3C), the model failed to meet all the qualitative criteria. Specifically, the virus only decayed to a post-treatment set point, instead of rebounding during the first treatment cycle. Furthermore, the viral response to the third treatment cycle was largely lost. This result suggests that immune regulation is required in order to represent the short-term (within treatment cycle) viral rebound dynamics. The model without drug tolerance (model #1, Fig 3B) and the model without viral escape (model #3, Fig 3D) both met all three qualitative requirements. The viral trajectories of these two models were comparable to the full model. However, removing both drug tolerance and viral escape (model #4, Fig 3E) resulted in virus that had an identical response in the third treatment cycle as it did in the first. This implies that either of these two mechanisms could have accounted for the long-term changes in viral response. The higher NLL and AIC for the model without drug tolerance (model #1 compared to model #3 without viral escape) was due to a poorer fit to the $CD8^+$ T cell and NK cell dynamics (Fig 4).

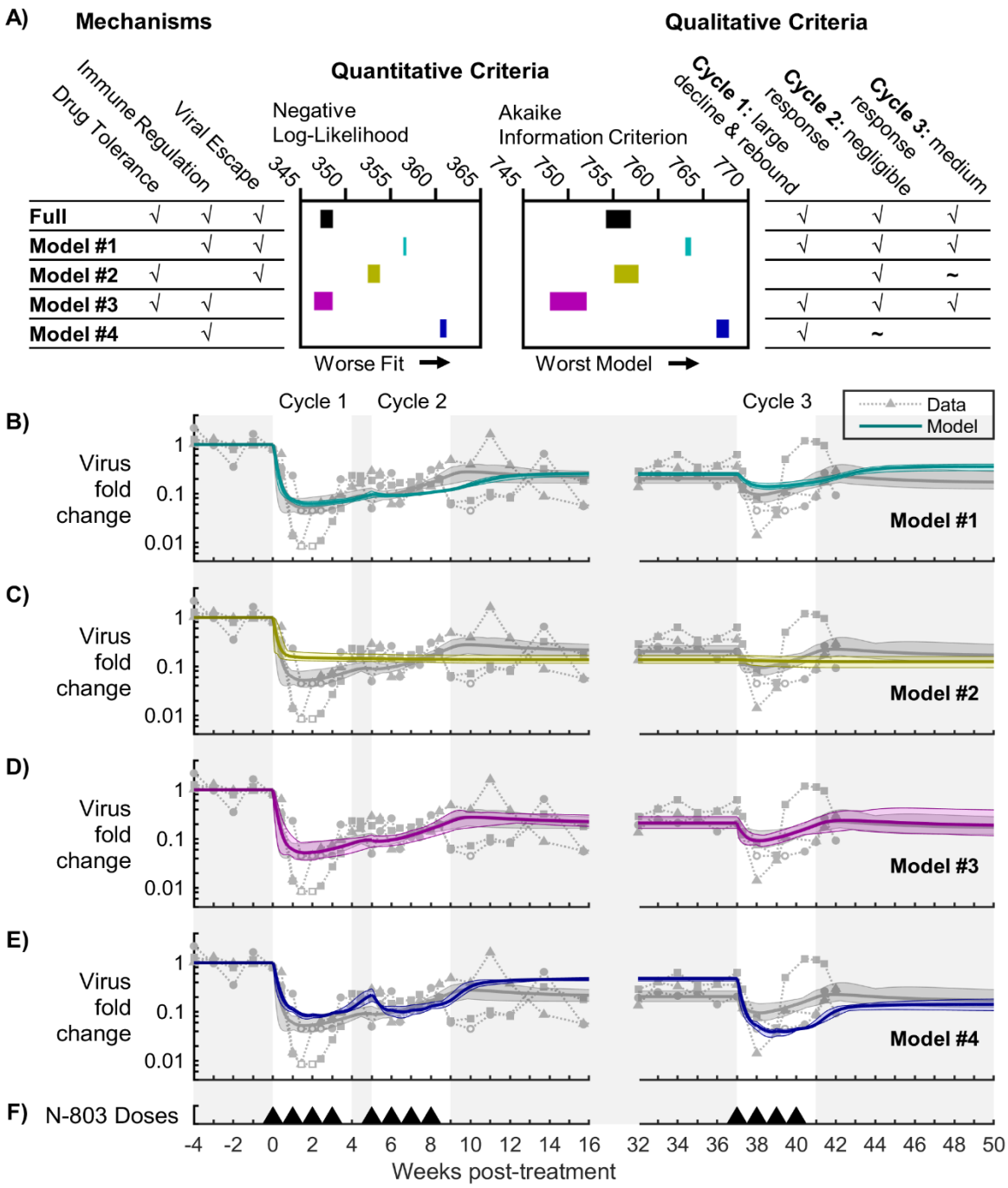

Fig 3. Model comparison for viral load. The calibration procedure was repeated for models with different combinations of mechanisms. Panel (A) shows the negative log-likelihood (NLL) and Akaike information criterion (AIC) for the top 20 calibrated parameter sets from each model, along with a checklist of qualitative criteria. Panels (B-E) compare the fold change in virus between the full model and models #1-4, respectively. Panel (F) shows timing of 0.1 mg/kg subcutaneous doses of N-803. Model outputs are shown as the mean (solid line) and range (shaded region) of model outputs from the top 20 parameter sets (lowest NLL) from the calibration procedure. Methodological details and fitted parameter values are given in S1 Appendix. Data from N-803-treated SIV-infected NHPs are shown as different symbols for each NHP [16]. Open symbols represent viral load below the detection limit of the assay (100 viral RNA copies/mL).

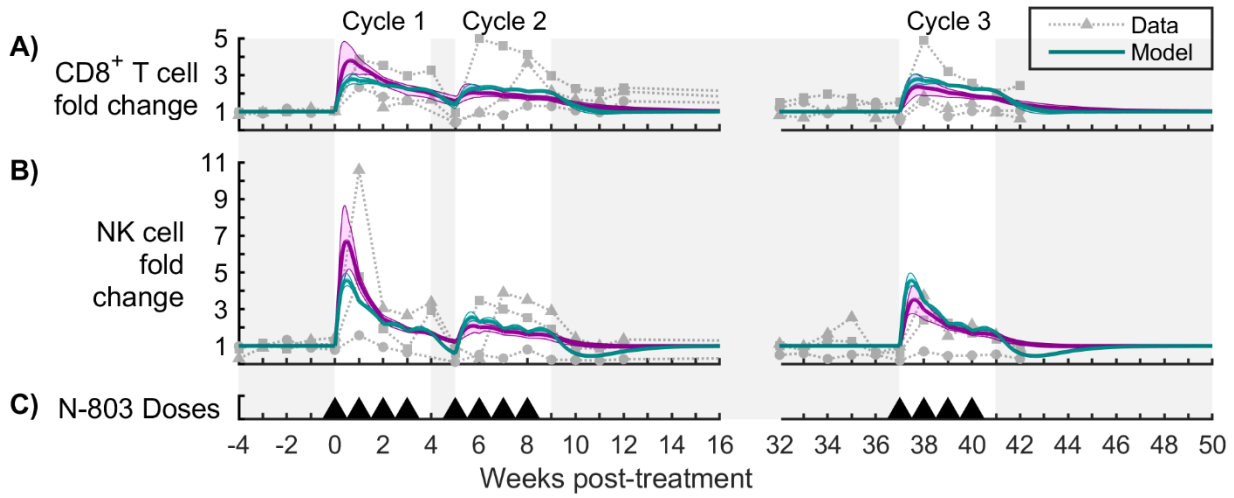

Fig 4. Model comparison for cytotoxic cells. Panels (A,B) show fold change in CD8⁺ T cells and NK cells in the peripheral blood, respectively, for the model without drug tolerance (cyan model #1) and the model without viral escape (magenta model #3). Results for model #2 were similar to model #3, and results for model #4 were similar to model #1 (see Fig S1). Panel (C) shows timing of 0.1 mg/kg subcutaneous doses of N-803. Model outputs are shown as the mean (solid line) and range (shaded region) of model outputs from the top 20 parameter sets (lowest NLL) from the calibration procedure. Methodological details and fitted parameter values are given in S1 Appendix. Data from N-803-treated SIV-infected NHPs are shown as different symbols for each NHP [16].

Model quantifies substantial loss in per-cell cytotoxic activity during the course of N-803 treatment.

We used the two minimal models (model #1 with immune regulation and viral escape; model #3 with immune regulation and drug tolerance) to quantify the timing and strengths of drug tolerance, immune regulation, and viral escape required to reproduce the observed viral dynamics during N-803 treatment. To this end, we defined a per-cell killing (PCK) metric that can be calculated from fitted parameter values (Eq. S11-S13 in S1 Appendix). The PCK is mathematically equivalent to the average rate of killing per infected cell per cytotoxic cell. In other words, multiplying the PCK by the sum of the cytotoxic cells (CD8⁺ T cells, E, and NK cells, K) and the sum of infected cells (both viral variants, I_V and I_W) will yield the total rate of loss of infected cells due to cytolytic action. The fold change in PCK due to immune regulation (Eq. S14) was quantified by the ratio of per-cell killing with immune regulation to the PCK without immune regulation (PCK(λ=0)). The effect of drug tolerance on PCK (Eq. S15) and the effect of viral escape on PCK (Eq. S16) were defined similarly.

Despite a brief increase in PCK, both models predict a significant reduction in per cell killing capacity by week 2 (Figs 5A,6A). Relative to pre-treatment values, PCK fell by 0.90-1.49 log in model #1 and 0.39-0.89 log in model #3, allowing the viral load to rebound within the first treatment cycle while $CD8^+$ T cells and NK cells were still elevated (Fig 4). Immune regulation caused a 0.43-0.76 log reduction in PCK in model #1 (Fig 5B) and a 0.40-1.66 log reduction in model #3 (Fig 6B). Both models predict a recovery in PCK after treatment cycles (week 4 and week 9), which coincided with recovery from immune regulation. Thus, immune regulation both strongly inhibited cytotoxicity during treatment (minimally ~0.4 log reduction) and quickly abated as the cytotoxic cell population normalized after treatment, precluding a post-treatment surge in viremia.

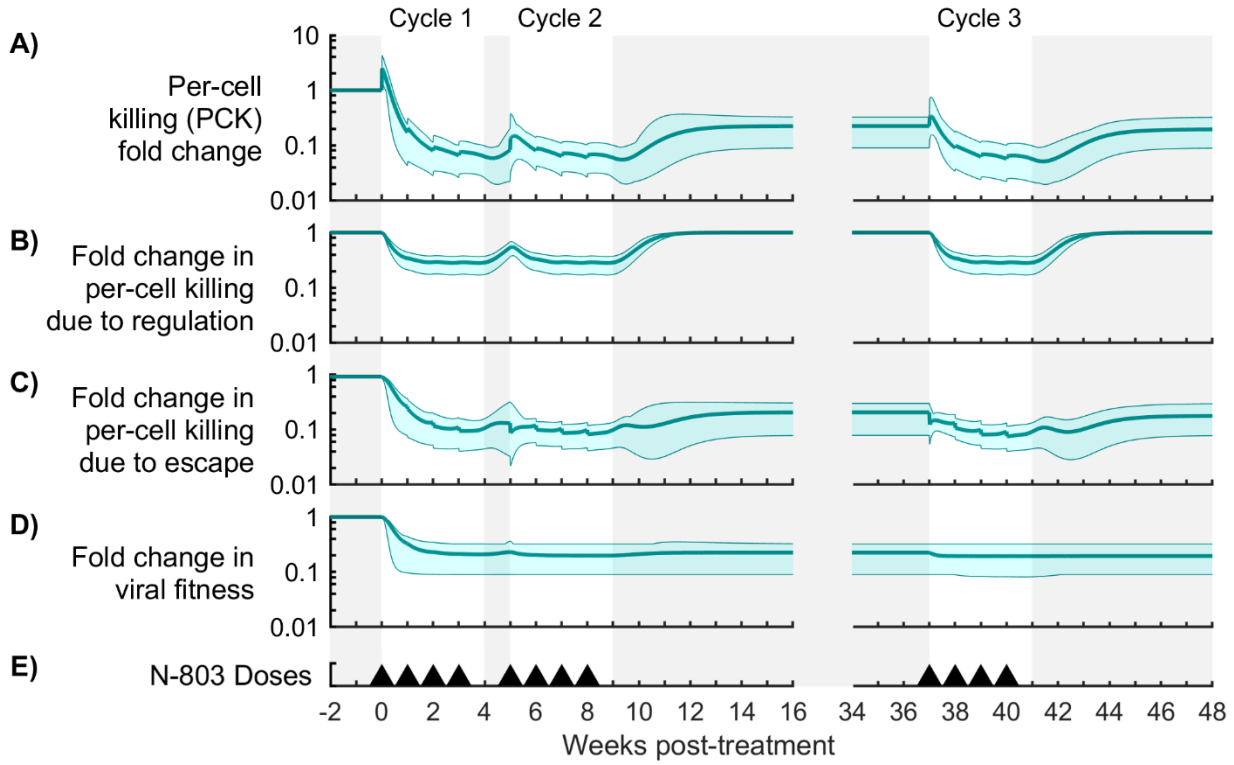

Fig 5. Contributions of immune regulation and viral escape to per-cell killing (PCK) for Model #1. Shown are measures of mechanism contribution for the model with immune regulation and viral escape (model #1). Panel (A) shows the fold change in per-cell killing rate, or PCK (Eq. S11-S13 in S1 Appendix). Panels (B,C) show the effect of immune regulation and viral escape on PCK (Eq. S14,S16). Panel (D) shows a measure of viral fitness (Eq. S17). Panel (E) shows timing of 0.1 mg/kg subcutaneous doses of N-803. Model outputs are shown as the mean (solid line) and range (shaded region) of model outputs from the top 20 parameter sets (lowest NLL) from the calibration procedure. Methodological details and fitted parameter values are given in S1 Appendix.

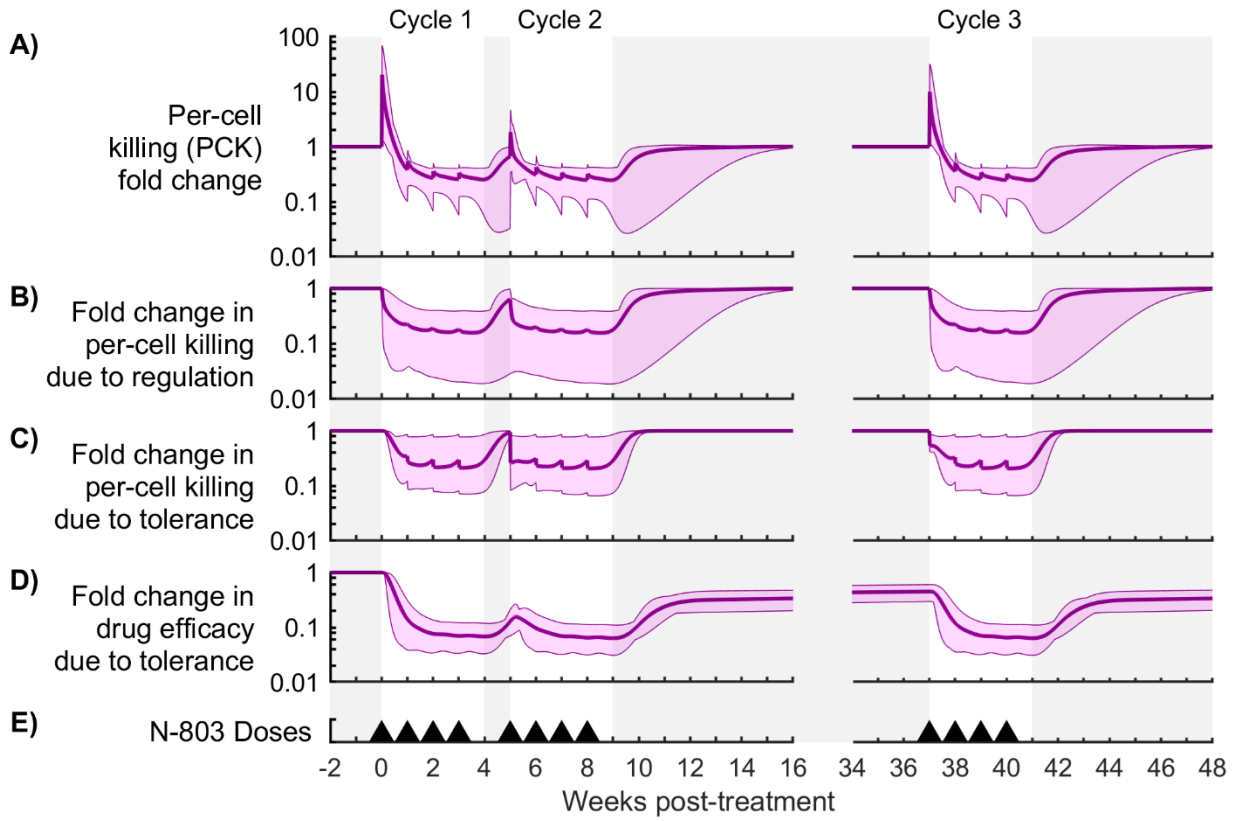

Fig 6. Contributions of immune regulation and drug tolerance to per-cell killing (PCK) for Model #3. Shown are measures of mechanism contribution for the model with immune regulation and drug tolerance (model #3). Panel (A) shows the fold change in per-cell killing rate, or PCK (Eq. S11-S13 in S1 Appendix). Panels (B,C) show the effect of immune regulation and drug tolerance on PCK (Eq. S14, S15). Panel (D) shows the effect of tolerance on drug efficacy (Eq. S13). Panel (E) shows timing of 0.1 mg/kg subcutaneous doses of N-803. Model outputs are shown as the mean (solid line) and range (shaded region) of model outputs from the top 20 parameter sets (lowest NLL) from the calibration procedure. Methodological details and fitted parameter values are given in S1 Appendix.

In model #1, viral escape reduced PCK more strongly (0.79-1.35 log reduction, Fig 5C) as compared to immune regulation. Viral escape was also more persistent, maintaining PCK at 0.53-1.11 log below pre-treatment killing rates between cycles 2 and 3 (Fig 5A). This escape from the $CD8^+$ T cell response was accompanied by a balancing reduction in viral fitness, which was estimated from the model by the fold change in the total viral proliferation rate (Fig 5D, Eq. S17). In model #3, drug tolerance reduced $CD8^+$ T cell and NK cell proliferation by 0.55-0.85 log (Fig S2), while its effect on PCK was indeterminant (0.11-1.12 log reduction, Fig 6C). A fraction of drug tolerance persisted across the treatment gap between cycles 2 and 3 (Fig. 6D), resulting in the first dose of cycle 3 (week 37) being 40-70% less effective than the first dose of cycle 1. Thus, drug tolerance reduced viral suppression in cycle 3 largely by modulating the proliferative

response of $CD8^+$ T cells and NK cells to N-803. These and other observations from the calibrated models were also supported by global sensitivity analysis (see S1 Appendix). The timing of immune regulation and drug tolerance in the model is reasonably consistent with expression of inhibitory markers (PD-1 and CD39) and IL-15 receptor subunits (CD122 and CD132) (further details in S1 Appendix).

N-803 treatment outcome can be improved by larger dosing periods and simultaneous regulatory blockade.

To test if the effects of immune regulation, drug tolerance, and viral escape can be overcome through treatment regimen changes, we predicted the impact of dosing periods and combination therapy on N-803 efficacy. We used both model #1 (immune regulation and viral escape) and model #3 (immune regulation and drug tolerance). Two treatment alternatives were tested: increasing time between doses; and blocking immune regulatory pathways.

Delivering 0.1 mg/kg subcutaneous N-803 doses at 2, 3, and 4 weeks apart yielded lower viral loads in both models, as compared to the current 1-week regimen (Figs 7A, S3A, and S4A). Delivering doses 4 weeks apart resulted in a post-treatment viral load that was, on average, 0.55 log below that of the original regimen for the model #1 and 2.04 log below for model #3. Dose spacing provided the greatest benefit in model #3 because longer windows between doses allowed more time for immune regulation and drug tolerance to abate (Figs S4B and S4C). In model #1, similar recovery from immune regulation was observed (Fig S3B), but treatment still ultimately resulted in selection of the T cell escape variant (Fig S3C). Taken together this indicates that dosing frequency changes are most likely to improve treatment outcomes if drug tolerance plays a significant part in the observed long-term NHP viral responses.

The second regimen change we explored was to reduce the killing regulation parameter (λ) to reflect the potential addition of a drug that blocks regulatory pathways (e.g. PD-1 or PD-L1 antagonists [52-55]). Reducing killing regulation (λ) by 40, 70, and 90% resulted in lower viral loads in both models (Figs 7B, S3D, and S4D). A 40% reduction in λ resulted in a 0.51 log lower average post-treatment viral load for model #1, compared to the original regimen, and a 1.08 log lower viral load for model #3. For model #3, the impact of reducing killing regulation was greater for cases when regulation acted early in the treatment cycle (Fig S4D). In model #1, increasing regulatory blockade yielded only small changes in the early viral reduction (Fig S3D) and hastened selection for T cell resistance (Fig S3F). However, inhibiting immune regulation by 70%

was sufficient to preclude viral rebound during weekly N-803 doses in both models (Fig S3D and S4D). In summary, blockade of immune regulation was consistently effective during weekly N-803 treatment in both models, but, if viral escape is limited (as assumed in model #3), it is especially effective early in the dosing period. Biologically, viral escape could be limited if the $CD8^+$ T cell responses are targeted to conserved viral epitopes [56, 57].

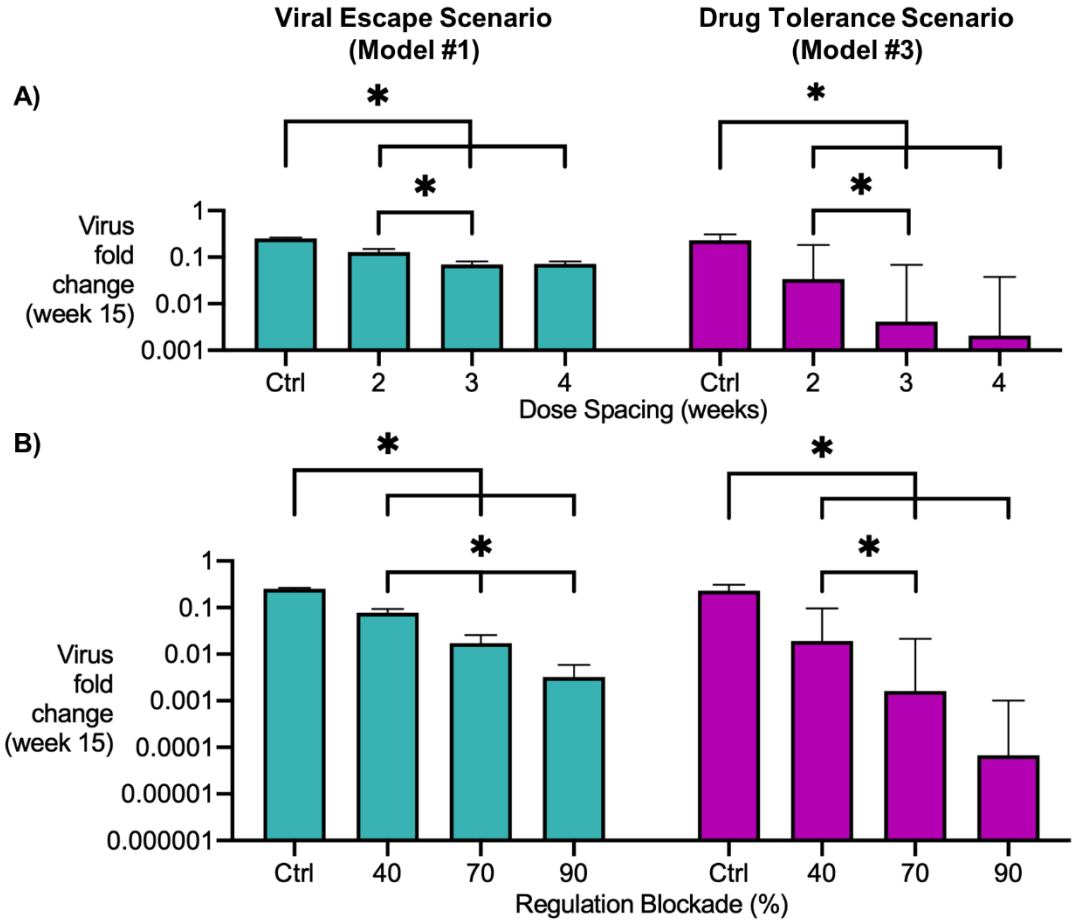

Fig 7. Potential for regimen changes to improve N-803 treatment outcome. Shown is a summary of the results of treatment exploration for both the model with immune regulation and viral escape (model #1, left column) and the model with immune regulation and drug tolerance (model #3, right column). Panel (A) shows the fold change in viral load at week 15 for regimens with different dose spacing: 1-week control regimen (Fig 2D) as well as 2-, 3-, and 4-week regimens. Panel (B) shows the fold change in viral load at week 15 for the 1-week regimen (Fig 2D) with different amounts of regulatory blockade (% reductions of killing regulation parameter λ): 0% control as well as 40, 70 and 90%. Model outputs are shown as the mean (column) and upper range (whisker) of model outputs from the top 20 parameter sets (lowest NLL) from the calibration procedure. ANOVA was performed as described in S1 Methods Appendix. Statistically significant differences between treatment changes and control, as well as between each successive treatment change, are marked ($P \leq 0.01$).

Discussion

We presented novel mathematical models representing immunotherapy of HIV through cytotoxic cell stimulation with an IL-15 superagonist (N-803). We combined the pharmacokinetics and pharmacodynamics of N-803 with an HIV infection model that includes cytotoxic T-cell and NK cell populations as well as experimentally identified mechanisms that lower N-803 efficacy: drug tolerance, immune regulation, and viral escape. The models were applied to analyze data collected from NHPs infected with SIV and treated with three cycles of N-803 [16]. The models reproduced key aspects of the viral and cytotoxic cell trajectories measured in the NHPs, including the transient suppression of viral load with weekly dosing and the partial recovery of drug efficacy following a 29 week break in treatment. Our models predicted how the cytotoxic effector functions of $CD8^+$ T cells and NK cells were diminished during treatment, resulting in rebound of the viral load during treatment. Model comparison suggested that immune regulatory pathways played an important role in the suppression of cytotoxic activity, as this mechanism was required for the model to reproduce viral dynamics in the first treatment cycle. Either drug tolerance or viral escape (or some combination thereof) were capable of accounting for the diminished response of the viral load to the third treatment cycle (relative to the first). The models predicted that adjusting the dosing period of N-803 or complementing with regulatory blockade could improve treatment outcomes. However, the ultimate effectiveness of N-803 monotherapy could be limited by viral escape from the $CD8^+$ T cell response.

We investigated two approaches to countermanding regulatory signals during N-803 treatment. First, we predict that simultaneous blockade of regulatory signals, along with N-803 treatment, could preclude the viral rebound observed during a weekly N-803 regimen, even if viral escape from the $CD8^+$ T cell response is a strong factor. Such combination of PD-1/PD-L1 blockade and an IL-15 agonist has shown promise against cancer in vitro [55]. Furthermore, blockade of the PD-1 pathway via anti-PD-1 or anti-PD-L1 antibodies in the absence of N-803 improved $CD8^+$ T cell function and reduced viral load in SIV-infected NHPs [52, 53] and increased HIV-1-specific $CD8^+$ T cell cytotoxicity in some participants in a clinical trial [54]. Our results suggest that IL-15-superagonist and PD-1/PD-L1 blockade combination therapy could be effective against HIV. The second method of countermanding regulation is extending the length of time between N-803 doses. Our model indicates that, when initiating N-803 treatment, there may be a period of cytotoxic stimulation before immune suppression. If subsequent doses are administered after the regulatory signal has abated, stronger efficacy can be achieved for each dose. Rigorous dosing optimization would require a model with more detailed representation of regulatory pathways such

as PD-1, as well as experimental data that frequently measures inhibitory marker dynamics during the critical first week after an N-803 dose. Nonetheless, our model indicates that doses spaced at least 2 weeks apart could improve N-803 efficacy.

N-803 immunotherapy may be perturbing the disease system in ways that persist long term, as evidenced by changes in the proliferative response of NK cells in the third cycle of treatment (drug tolerance) and by changes in the sequences of $CD8^+$ T cell epitopes in the viral population (viral escape) [16]. Our model demonstrated that long-term changes could be the result of either or both of these phenomena. Further studies will be needed to better quantify the relative contribution of drug tolerance and viral escape in NHPs, and these contributions will affect further N-803 treatment development. If drug tolerance is the main driving mechanism behind the long-term response to N-803 treatment, the effect of tolerance may be circumvented with an optimized dosing regimen. In contrast, while viral escape did not completely preclude a successful N-803 regimen, it limited the impact of all treatment changes (compare model #3 to model #1). There may be a need to couple N-803 with a vaccine that elicits $CD8^+$ T cells responses targeting conserved viral epitopes. It was postulated that the viral suppression observed in the NHPs used for this study was enabled by the vaccine status of the animals [16]. In ART-treated, SIV-infected NHPs, delivering either therapeutic vaccines [58] or broadly neutralizing antibodies (bnAbs) [59], in combination with an activator (a TLR7 agonist), delayed viral rebound after ART cessation. Additionally, N-803 was shown to enhanced antibody dependent cell-mediated cytotoxicity (ADCC) in NK cells against human cancer cells [60], suggesting a potential for synergy with bnAbs.

The linchpin of treating HIV via stimulation of cytotoxic cells is that cytotoxic cells need to find infected cells. Infected cells can evade detection by either not actively producing virions (latent infection [3, 61, 62]) or by existing in immune privileged tissues (e.g. central nervous system [63] or B-cell follicles in lymph nodes [64]). N-803 has interesting properties regarding both of these mechanisms that could be incorporated in more comprehensive future models. First, N-803 is a latency reversing agent [65, 66], which was neglected in our model. Reactivation of latent infections may have contributed to viral rebound and escape in the N-803 treated NHPs. Furthermore, the addition of PD-1 blockade, as discussed earlier, could enhance the latency reversing effect [67]. Including a latency mechanism would allow the model to more explicitly address these phenomena and inform the degree to which N-803 could reduce the latent reservoir. Second, N-803 also induces cytotoxic T-cell migration into lymph tissue and B-cell

follicles [15]. Our current model does not account for trafficking between blood and lymph tissue, though N-803-induced migration of $CD8^+$ T cells into B-cell follicles is phenomenologically represented by increases in killing rate according to parameters γ_E,γ_K (Eq. 7). Increased trafficking out of the blood may also have accounted for some of the observed contraction in peripheral blood $CD8^+$ T cells and NK cells in our NHP data. The importance of these phenomena could be more explicitly addressed by expanding the current model to include lymph node dynamics. This would allow us to ascertain how the currently predicted results from treatment improvements would translate into cloistered compartments, allowing for a better estimation of the effect of N-803 on the total body viremia.

Our model could be adapted and calibrated to data from different NHP cohorts, comparing SIV controllers and progressors or comparing N-803 responders and non-responders. While N-803 treatment reduced the plasma SIV load in our NHPs [16], similar reductions of SIV in the plasma were not consistently demonstrated in other studies using N-803 [15] or monomeric IL-15 [9, 10]. This may be because our cohort was predisposed to SIV control, which could be due to multiple factors. For example, both the Mamu-B*08 allele [68] and the Mamu-B*17 allele [69] are associated with better immune control of SIV in rhesus macaques. Beyond MHC expression, there is also evidence that $CD8^+$ T cells of human elite controllers have transcriptional signatures that favor cytokine expression over cytolytic functions, as compared to $CD8^+$ T cells from chronic progressors [70]. Mechanisms behind elite control of SIV/HIV still need to be elucidated by further experimental and modeling studies. Future mathematical models could evaluate the possible influence of MHC alleles and $CD8^+$ functionality in driving differences between these groups.

In summary, we developed and analyzed a mathematical model to help decode the complex immune interactions induced by N-803-therapy of HIV. This work will inform not only N-803 treatment but also its potential combination with other immune therapies and ART toward a functional cure for HIV.

Acknowledgments

We thank ImmunityBio for supplying the reagent N-803.

References

1. UNAIDS. UNAIDS DATA 2020: UNAIDS; 2020 [cited 2018 9/2/2020]. Available from: https://www.unaids.org/sites/default/files/media_asset/2020_aids-data-book_en.pdf.
2. Etemad B, Esmaeilzadeh E, Li JZ. Learning From the Exceptions: HIV Remission in Post-treatment Controllers. Frontiers in immunology. 2019;10:1749. Epub 2019/08/10. doi: 10.3389/fimmu.2019.01749. PubMed PMID: 31396237; PubMed Central PMCID: PMCPMC6668499.
3. Thorlund K, Horwitz MS, Fife BT, Lester R, Cameron DW. Landscape review of current HIV 'kick and kill' cure research - some kicking, not enough killing. BMC infectious diseases. 2017;17(1):595. Epub 2017/08/31. doi: 10.1186/s12879-017-2683-3. PubMed PMID: 28851294; PubMed Central PMCID: PMCPMC5576299.
4. Perreau M, Banga R, Pantaleo G. Targeted Immune Interventions for an HIV-1 Cure. Trends in molecular medicine. 2017;23(10):945-61. Epub 2017/09/12. doi: 10.1016/j.molmed.2017.08.006. PubMed PMID: 28890135.
5. Saeidi A, Zandi K, Cheok YY, Saeidi H, Wong WF, Lee CYQ, et al. T-Cell Exhaustion in Chronic Infections: Reversing the State of Exhaustion and Reinvigorating Optimal Protective Immune Responses. Frontiers in immunology. 2018;9:2569. Epub 2018/11/27. doi: 10.3389/fimmu.2018.02569. PubMed PMID: 30473697; PubMed Central PMCID: PMCPMC6237934.
6. Ram DR, Manickam C, Lucar O, Shah SV, Reeves RK. Adaptive NK cell responses in HIV/SIV infections: A roadmap to cell-based therapeutics? Journal of leukocyte biology. 2019;105(6):1253-9. Epub 2019/02/08. doi: 10.1002/jlb.Mr0718-303r. PubMed PMID: 30730588; PubMed Central PMCID: PMCPMC6536345.
7. Robinson TO, Schluns KS. The potential and promise of IL-15 in immuno-oncogenic therapies. Immunology letters. 2017;190:159-68. Epub 2017/08/22. doi: 10.1016/j.imlet.2017.08.010. PubMed PMID: 28823521; PubMed Central PMCID: PMCPMC5774016.
8. Patidar M, Yadav N, Dalai SK. Interleukin 15: A key cytokine for immunotherapy. Cytokine & growth factor reviews. 2016;31:49-59. Epub 2016/06/22. doi: 10.1016/j.cytogfr.2016.06.001. PubMed PMID: 27325459.
9. Mueller YM, Petrovas C, Bojczuk PM, Dimitriou ID, Beer B, Silvera P, et al. Interleukin-15 increases effector memory CD8+ t cells and NK Cells in simian immunodeficiency virus-infected macaques. Journal of virology. 2005;79(8):4877-85. Epub 2005/03/30.

doi: 10.1128/jvi.79.8.4877-4885.2005. PubMed PMID: 15795273; PubMed Central PMCID: PMCPMC1069542.

10. Mueller YM, Do DH, Altork SR, Artlett CM, Gracely EJ, Katsetos CD, et al. IL-15 treatment during acute simian immunodeficiency virus (SIV) infection increases viral set point and accelerates disease progression despite the induction of stronger SIV-specific CD8+ T cell responses. Journal of immunology (Baltimore, Md : 1950). 2008;180(1):350-60. Epub 2007/12/22. doi: 10.4049/jimmunol.180.1.350. PubMed PMID: 18097036; PubMed Central PMCID: PMCPMC2929904.
11. Watson DC, Moysi E, Valentin A, Bergamaschi C, Devasundaram S, Fortis SP, et al. Treatment with native heterodimeric IL-15 increases cytotoxic lymphocytes and reduces SHIV RNA in lymph nodes. PLoS pathogens. 2018;14(2):e1006902. Epub 2018/02/24. doi: 10.1371/journal.ppat.1006902. PubMed PMID: 29474450; PubMed Central PMCID: PMCPMC5825155.
12. Zhu X, Marcus WD, Xu W, Lee HI, Han K, Egan JO, et al. Novel human interleukin-15 agonists. Journal of immunology (Baltimore, Md : 1950). 2009;183(6):3598-607. Epub 2009/08/28. doi: 10.4049/jimmunol.0901244. PubMed PMID: 19710453; PubMed Central PMCID: PMCPMC2814526.
13. Stoklasek TA, Schluns KS, Lefrançois L. Combined IL-15/IL-15Ralpha immunotherapy maximizes IL-15 activity in vivo. Journal of immunology (Baltimore, Md : 1950). 2006;177(9):6072-80. Epub 2006/10/24. doi: 10.4049/jimmunol.177.9.6072. PubMed PMID: 17056533; PubMed Central PMCID: PMCPMC2847275.
14. Rhode PR, Egan JO, Xu W, Hong H, Webb GM, Chen X, et al. Comparison of the Superagonist Complex, ALT-803, to IL15 as Cancer Immunotherapeutics in Animal Models. Cancer immunology research. 2016;4(1):49-60. Epub 2015/10/30. doi: 10.1158/2326-6066.cir-15-0093-t. PubMed PMID: 26511282; PubMed Central PMCID: PMCPMC4703482.
15. Webb GM, Li S, Mwakalundwa G, Folkvord JM, Greene JM, Reed JS, et al. The human IL-15 superagonist ALT-803 directs SIV-specific CD8(+) T cells into B-cell follicles. Blood advances. 2018;2(2):76-84. Epub 2018/01/25. doi: 10.1182/bloodadvances.2017012971. PubMed PMID: 29365313; PubMed Central PMCID: PMCPMC5787870.
16. Ellis-Connell AL, Balgeman AJ, Zarbock KR, Barry G, Weiler A, Egan JO, et al. ALT-803 Transiently Reduces Simian Immunodeficiency Virus Replication in the Absence of Antiretroviral Treatment. Journal of virology. 2018;92(3). Epub 2017/11/10. doi:

10.1128/jvi.01748-17. PubMed PMID: 29118125; PubMed Central PMCID: PMCPMC5774892.

17. Wrangle JM, Velcheti V, Patel MR, Garrett-Mayer E, Hill EG, Ravenel JG, et al. ALT-803, an IL-15 superagonist, in combination with nivolumab in patients with metastatic non-small cell lung cancer: a non-randomised, open-label, phase 1b trial. The Lancet Oncology. 2018;19(5):694-704. Epub 2018/04/10. doi: 10.1016/s1470-2045(18)30148-7. PubMed PMID: 29628312; PubMed Central PMCID: PMCPMC6089612.
18. Romee R, Cooley S, Berrien-Elliott MM, Westervelt P, Verneris MR, Wagner JE, et al. First-in-human phase 1 clinical study of the IL-15 superagonist complex ALT-803 to treat relapse after transplantation. Blood. 2018;131(23):2515-27. Epub 2018/02/22. doi: 10.1182/blood-2017-12-823757. PubMed PMID: 29463563; PubMed Central PMCID: PMCPMC5992862.
19. Margolin K, Morishima C, Velcheti V, Miller JS, Lee SM, Silk AW, et al. Phase I Trial of ALT-803, A Novel Recombinant IL15 Complex, in Patients with Advanced Solid Tumors. Clinical cancer research : an official journal of the American Association for Cancer Research. 2018. Epub 2018/07/27. doi: 10.1158/1078-0432.Ccr-18-0945. PubMed PMID: 30045932.
20. Kim PS, Kwilas AR, Xu W, Alter S, Jeng EK, Wong HC, et al. IL-15 superagonist/IL-15RalphaSushi-Fc fusion complex (IL-15SA/IL-15RalphaSu-Fc; ALT-803) markedly enhances specific subpopulations of NK and memory CD8+ T cells, and mediates potent anti-tumor activity against murine breast and colon carcinomas. Oncotarget. 2016;7(13):16130-45. Epub 2016/02/26. doi: 10.18632/oncotarget.7470. PubMed PMID: 26910920; PubMed Central PMCID: PMCPMC4941302.
21. Burrack KS, Huggins MA, Taras E, Dougherty P, Henzler CM, Yang R, et al. Interleukin-15 Complex Treatment Protects Mice from Cerebral Malaria by Inducing Interleukin-10-Producing Natural Killer Cells. Immunity. 2018;48(4):760-72.e4. Epub 2018/04/08. doi: 10.1016/j.immuni.2018.03.012. PubMed PMID: 29625893; PubMed Central PMCID: PMCPMC5906161.
22. Phillips RE, Rowland-Jones S, Nixon DF, Gotch FM, Edwards JP, Ogunlesi AO, et al. Human immunodeficiency virus genetic variation that can escape cytotoxic T cell recognition. Nature. 1991;354(6353):453-9. Epub 1991/12/12. doi: 10.1038/354453a0. PubMed PMID: 1721107.

23. Goulder PJ, Watkins DI. HIV and SIV CTL escape: implications for vaccine design. Nature reviews Immunology. 2004;4(8):630-40. Epub 2004/08/03. doi: 10.1038/nri1417. PubMed PMID: 15286729.

24. Allen TM, O'Connor DH, Jing P, Dzuris JL, Mothé BR, Vogel TU, et al. Tat-specific cytotoxic T lymphocytes select for SIV escape variants during resolution of primary viraemia. Nature. 2000;407(6802):386-90. Epub 2000/10/03. doi: 10.1038/35030124. PubMed PMID: 11014195.

25. Padmanabhan P, Dixit NM. Models of Viral Population Dynamics. Current topics in microbiology and immunology. 2016;392:277-302. Epub 2015/07/16. doi: 10.1007/82_2015_458. PubMed PMID: 26174625.

26. Perelson AS, Ribeiro RM. Modeling the within-host dynamics of HIV infection. BMC biology. 2013;11:96. Epub 2013/09/12. doi: 10.1186/1741-7007-11-96. PubMed PMID: 24020860; PubMed Central PMCID: PMCPMC3765939.

27. Banks HT, Flores KB, Hu S, Rosenberg E, Buzon M, Yu X, et al. Immuno-modulatory strategies for reduction of HIV reservoir cells. Journal of theoretical biology. 2015;372:146-58. Epub 2015/02/24. doi: 10.1016/j.jtbi.2015.02.006. PubMed PMID: 25701451; PubMed Central PMCID: PMCPMC4390551.

28. Petravic J, Martyushev A, Reece JC, Kent SJ, Davenport MP. Modeling the timing of antilatency drug administration during HIV treatment. Journal of virology. 2014;88(24):14050-6. Epub 2014/09/26. doi: 10.1128/jvi.01701-14. PubMed PMID: 25253352; PubMed Central PMCID: PMCPMC4249129.

29. Althaus CL, De Boer RJ. Dynamics of immune escape during HIV/SIV infection. PLoS computational biology. 2008;4(7):e1000103. Epub 2008/07/19. doi: 10.1371/journal.pcbi.1000103. PubMed PMID: 18636096; PubMed Central PMCID: PMCPMC2423483.

30. Simonov M, Rawlings RA, Comment N, Reed SE, Shi X, Nelson PW. Modeling adaptive regulatory T-cell dynamics during early HIV infection. PloS one. 2012;7(4):e33924. Epub 2012/04/27. doi: 10.1371/journal.pone.0033924. PubMed PMID: 22536321; PubMed Central PMCID: PMCPMC3334930.

31. Wendelsdorf K, Dean G, Hu S, Nordone S, Banks HT. Host immune responses that promote initial HIV spread. Journal of theoretical biology. 2011;289:17-35. Epub 2011/08/30. doi: 10.1016/j.jtbi.2011.08.012. PubMed PMID: 21871901; PubMed Central PMCID: PMCPMC3191247.

32. Read EL, Tovo-Dwyer AA, Chakraborty AK. Stochastic effects are important in intrahost HIV evolution even when viral loads are high. Proceedings of the National Academy of Sciences of the United States of America. 2012;109(48):19727-32. Epub 2012/11/01. doi: 10.1073/pnas.1206940109. PubMed PMID: 23112156; PubMed Central PMCID: PMCPMC3511713.

33. Cardozo EF, Andrade A, Mellors JW, Kuritzkes DR, Perelson AS, Ribeiro RM. Treatment with integrase inhibitor suggests a new interpretation of HIV RNA decay curves that reveals a subset of cells with slow integration. PLoS pathogens. 2017;13(7):e1006478. Epub 2017/07/06. doi: 10.1371/journal.ppat.1006478. PubMed PMID: 28678879; PubMed Central PMCID: PMCPMC5513547.

34. Conway JM, Perelson AS. Residual Viremia in Treated HIV+ Individuals. PLoS computational biology. 2016;12(1):e1004677. Epub 2016/01/07. doi: 10.1371/journal.pcbi.1004677. PubMed PMID: 26735135; PubMed Central PMCID: PMCPMC4703306.

35. Martins MA, Tully DC, Cruz MA, Power KA, Veloso de Santana MG, Bean DJ, et al. Vaccine-Induced Simian Immunodeficiency Virus-Specific CD8+ T-Cell Responses Focused on a Single Nef Epitope Select for Escape Variants Shortly after Infection. Journal of virology. 2015;89(21):10802-20. Epub 2015/08/21. doi: 10.1128/jvi.01440-15. PubMed PMID: 26292326; PubMed Central PMCID: PMCPMC4621113.

36. Asquith B, Edwards CT, Lipsitch M, McLean AR. Inefficient cytotoxic T lymphocyte-mediated killing of HIV-1-infected cells in vivo. PLoS biology. 2006;4(4):e90. Epub 2006/03/07. doi: 10.1371/journal.pbio.0040090. PubMed PMID: 16515366; PubMed Central PMCID: PMCPMC1395353.

37. Asquith B, McLean AR. In vivo CD8+ T cell control of immunodeficiency virus infection in humans and macaques. Proceedings of the National Academy of Sciences of the United States of America. 2007;104(15):6365-70. Epub 2007/04/04. doi: 10.1073/pnas.0700666104. PubMed PMID: 17404226; PubMed Central PMCID: PMCPMC1851058.

38. Friedrich TC, Dodds EJ, Yant LJ, Vojnov L, Rudersdorf R, Cullen C, et al. Reversion of CTL escape-variant immunodeficiency viruses in vivo. Nature medicine. 2004;10(3):275-81. Epub 2004/02/18. doi: 10.1038/nm998. PubMed PMID: 14966520.

39. Peut V, Kent SJ. Fitness constraints on immune escape from HIV: Implications of envelope as a target for both HIV-specific T cells and antibody. Current HIV research.

2006;4(2):191-7. Epub 2006/04/14. doi: 10.2174/157016206776055110. PubMed PMID: 16611057.

40. Arcia D, Acevedo-Saenz L, Rugeles MT, Velilla PA. Role of CD8(+) T Cells in the Selection of HIV-1 Immune Escape Mutations. Viral immunology. 2017;30(1):3-12. Epub 2016/11/03. doi: 10.1089/vim.2016.0095. PubMed PMID: 27805477.

41. Choo DK, Murali-Krishna K, Anita R, Ahmed R. Homeostatic turnover of virus-specific memory CD8 T cells occurs stochastically and is independent of CD4 T cell help. Journal of immunology (Baltimore, Md : 1950). 2010;185(6):3436-44. Epub 2010/08/25. doi: 10.4049/jimmunol.1001421. PubMed PMID: 20733203.

42. Hataye J, Moon JJ, Khoruts A, Reilly C, Jenkins MK. Naive and memory CD4+ T cell survival controlled by clonal abundance. Science (New York, NY). 2006;312(5770):114-6. Epub 2006/03/04. doi: 10.1126/science.1124228. PubMed PMID: 16513943.

43. Lutz CT, Karapetyan A, Al-Attar A, Shelton BJ, Holt KJ, Tucker JH, et al. Human NK cells proliferate and die in vivo more rapidly than T cells in healthy young and elderly adults. Journal of immunology (Baltimore, Md : 1950). 2011;186(8):4590-8. Epub 2011/03/16. doi: 10.4049/jimmunol.1002732. PubMed PMID: 21402893; PubMed Central PMCID: PMCPMC3071442.

44. Freitas AA, Rocha B. Population biology of lymphocytes: the flight for survival. Annual review of immunology. 2000;18:83-111. Epub 2000/06/03. doi: 10.1146/annurev.immunol.18.1.83. PubMed PMID: 10837053.

45. Banks HT, Davidian M, Hu S, Kepler GM, Rosenberg ES. Modelling HIV immune response and validation with clinical data. Journal of biological dynamics. 2008;2(4):357-85. Epub 2008/01/01. doi: 10.1080/17513750701813184. PubMed PMID: 19495424; PubMed Central PMCID: PMCPMC2689816.

46. Jambhekar SS, Breen PJ. Extravascular routes of drug administration. Basic Pharmacokinetics. 2 ed: Pharmaceutical Press; 2012. p. 105-26.

47. Fujii R, Jochems C, Tritsch SR, Wong HC, Schlom J, Hodge JW. An IL-15 superagonist/IL-15Rα fusion complex protects and rescues NK cell-cytotoxic function from TGF-β1-mediated immunosuppression. Cancer immunology, immunotherapy : CII. 2018;67(4):675-89. Epub 2018/02/03. doi: 10.1007/s00262-018-2121-4. PubMed PMID: 29392336; PubMed Central PMCID: PMCPMC6326360.

48. Rosario M, Liu B, Kong L, Collins LI, Schneider SE, Chen X, et al. The IL-15-Based ALT-803 Complex Enhances FcgammaRIIIa-Triggered NK Cell Responses and In

Vivo Clearance of B Cell Lymphomas. Clinical cancer research : an official journal of the American Association for Cancer Research. 2016;22(3):596-608. Epub 2015/10/02. doi: 10.1158/1078-0432.ccr-15-1419. PubMed PMID: 26423796; PubMed Central PMCID: PMCPMC4738096.

49. Basher F, Jeng EK, Wong H, Wu J. Cooperative therapeutic anti-tumor effect of IL-15 agonist ALT-803 and co-targeting soluble NKG2D ligand sMIC. Oncotarget. 2016;7(1):814-30. Epub 2015/12/02. doi: 10.18632/oncotarget.6416. PubMed PMID: 26625316; PubMed Central PMCID: PMCPMC4808035.

50. Bailey CP, Budak-Alpdogan T, Sauter CT, Panis MM, Buyukgoz C, Jeng EK, et al. New interleukin-15 superagonist (IL-15SA) significantly enhances graft-versus-tumor activity. Oncotarget. 2017;8(27):44366-78. Epub 2017/06/03. doi: 10.18632/oncotarget.17875. PubMed PMID: 28574833; PubMed Central PMCID: PMCPMC5546486.

51. Weninger W, Crowley MA, Manjunath N, von Andrian UH. Migratory properties of naive, effector, and memory CD8(+) T cells. The Journal of experimental medicine. 2001;194(7):953-66. Epub 2001/10/03. doi: 10.1084/jem.194.7.953. PubMed PMID: 11581317; PubMed Central PMCID: PMCPMC2193483.

52. Velu V, Titanji K, Zhu B, Husain S, Pladevega A, Lai L, et al. Enhancing SIV-specific immunity in vivo by PD-1 blockade. Nature. 2009;458(7235):206-10. Epub 2008/12/17. doi: 10.1038/nature07662. PubMed PMID: 19078956; PubMed Central PMCID: PMCPMC2753387.

53. Dyavar Shetty R, Velu V, Titanji K, Bosinger SE, Freeman GJ, Silvestri G, et al. PD-1 blockade during chronic SIV infection reduces hyperimmune activation and microbial translocation in rhesus macaques. The Journal of clinical investigation. 2012;122(5):1712-6. Epub 2012/04/24. doi: 10.1172/jci60612. PubMed PMID: 22523065; PubMed Central PMCID: PMCPMC3336983.

54. Gay CL, Bosch RJ, Ritz J, Hataye JM, Aga E, Tressler RL, et al. Clinical Trial of the Anti-PD-L1 Antibody BMS-936559 in HIV-1 Infected Participants on Suppressive Antiretroviral Therapy. The Journal of infectious diseases. 2017;215(11):1725-33. Epub 2017/04/22. doi: 10.1093/infdis/jix191. PubMed PMID: 28431010; PubMed Central PMCID: PMCPMC5790148.

55. Jochems C, Tritsch SR, Knudson KM, Gameiro SR, Rumfield CS, Pellom ST, et al. The multi-functionality of N-809, a novel fusion protein encompassing anti-PD-L1 and the IL-15 superagonist fusion complex. Oncoimmunology. 2019;8(2):e1532764. Epub

2019/02/05. doi: 10.1080/2162402x.2018.1532764. PubMed PMID: 30713787; PubMed Central PMCID: PMCPMC6343815.

56. Harris M, Burns CM, Becker EA, Braasch AT, Gostick E, Johnson RC, et al. Acute-phase CD8 T cell responses that select for escape variants are needed to control live attenuated simian immunodeficiency virus. Journal of virology. 2013;87(16):9353-64. Epub 2013/06/21. doi: 10.1128/jvi.00909-13. PubMed PMID: 23785211; PubMed Central PMCID: PMCPMC3754066.

57. Burwitz BJ, Sacha JB, Reed JS, Newman LP, Norante FA, Bimber BN, et al. Pyrosequencing reveals restricted patterns of CD8+ T cell escape-associated compensatory mutations in simian immunodeficiency virus. Journal of virology. 2011;85(24):13088-96. Epub 2011/10/14. doi: 10.1128/jvi.05650-11. PubMed PMID: 21994463; PubMed Central PMCID: PMCPMC3233179.

58. Borducchi EN, Cabral C, Stephenson KE, Liu J, Abbink P, Ng'ang'a D, et al. Ad26/MVA therapeutic vaccination with TLR7 stimulation in SIV-infected rhesus monkeys. Nature. 2016;540(7632):284-7. Epub 2016/11/15. doi: 10.1038/nature20583. PubMed PMID: 27841870; PubMed Central PMCID: PMCPMC5145754.

59. Borducchi EN, Liu J, Nkolola JP, Cadena AM, Yu WH, Fischinger S, et al. Antibody and TLR7 agonist delay viral rebound in SHIV-infected monkeys. Nature. 2018;563(7731):360-4. Epub 2018/10/05. doi: 10.1038/s41586-018-0600-6. PubMed PMID: 30283138; PubMed Central PMCID: PMCPMC6237629.

60. Fantini M, David JM, Wong HC, Annunziata CM, Arlen PM, Tsang KY. An IL-15 Superagonist, ALT-803, Enhances Antibody-Dependent Cell-Mediated Cytotoxicity Elicited by the Monoclonal Antibody NEO-201 Against Human Carcinoma Cells. Cancer biotherapy & radiopharmaceuticals. 2019;34(3):147-59. Epub 2019/01/03. doi: 10.1089/cbr.2018.2628. PubMed PMID: 30601063; PubMed Central PMCID: PMCPMC6482908.

61. Melkova Z, Shankaran P, Madlenakova M, Bodor J. Current views on HIV-1 latency, persistence, and cure. Folia microbiologica. 2017;62(1):73-87. Epub 2016/10/07. doi: 10.1007/s12223-016-0474-7. PubMed PMID: 27709447.

62. Pankrac J, Klein K, Mann JFS. Eradication of HIV-1 latent reservoirs through therapeutic vaccination. AIDS research and therapy. 2017;14(1):45. Epub 2017/09/13. doi: 10.1186/s12981-017-0177-4. PubMed PMID: 28893280; PubMed Central PMCID: PMCPMC5594457.

63. Salemi M, Rife B. Phylogenetics and Phyloanatomy of HIV/SIV Intra-Host Compartments and Reservoirs: The Key Role of the Central Nervous System. Current HIV research. 2016;14(2):110-20. Epub 2015/10/30. PubMed PMID: 26511341.

64. Bronnimann MP, Skinner PJ, Connick E. The B-Cell Follicle in HIV Infection: Barrier to a Cure. Frontiers in immunology. 2018;9:20. Epub 2018/02/10. doi: 10.3389/fimmu.2018.00020. PubMed PMID: 29422894; PubMed Central PMCID: PMCPMC5788973.

65. Jones RB, Mueller S, O'Connor R, Rimpel K, Sloan DD, Karel D, et al. A Subset of Latency-Reversing Agents Expose HIV-Infected Resting CD4+ T-Cells to Recognition by Cytotoxic T-Lymphocytes. PLoS pathogens. 2016;12(4):e1005545. Epub 2016/04/16. doi: 10.1371/journal.ppat.1005545. PubMed PMID: 27082643; PubMed Central PMCID: PMCPMC4833318.

66. McBrien JB, Mavigner M, Franchitti L, Smith SA, White E, Tharp GK, et al. Robust and persistent reactivation of SIV and HIV by N-803 and depletion of CD8(+) cells. Nature. 2020;578(7793):154-9. Epub 2020/01/24. doi: 10.1038/s41586-020-1946-0. PubMed PMID: 31969705.

67. Fromentin R, DaFonseca S, Costiniuk CT, El-Far M, Procopio FA, Hecht FM, et al. PD-1 blockade potentiates HIV latency reversal ex vivo in CD4(+) T cells from ART-suppressed individuals. Nature communications. 2019;10(1):814. Epub 2019/02/20. doi: 10.1038/s41467-019-08798-7. PubMed PMID: 30778080; PubMed Central PMCID: PMCPMC6379401.

68. Loffredo JT, Maxwell J, Qi Y, Glidden CE, Borchardt GJ, Soma T, et al. Mamu-B*08-positive macaques control simian immunodeficiency virus replication. Journal of virology. 2007;81(16):8827-32. Epub 2007/06/01. doi: 10.1128/jvi.00895-07. PubMed PMID: 17537848; PubMed Central PMCID: PMCPMC1951344.

69. Yant LJ, Friedrich TC, Johnson RC, May GE, Maness NJ, Enz AM, et al. The high-frequency major histocompatibility complex class I allele Mamu-B*17 is associated with control of simian immunodeficiency virus SIVmac239 replication. Journal of virology. 2006;80(10):5074-7. Epub 2006/04/28. doi: 10.1128/jvi.80.10.5074-5077.2006. PubMed PMID: 16641299; PubMed Central PMCID: PMCPMC1472056.

70. Nguyen S, Deleage C, Darko S, Ransier A, Truong DP, Agarwal D, et al. Elite control of HIV is associated with distinct functional and transcriptional signatures in lymphoid tissue CD8(+) T cells. Science translational medicine. 2019;11(523). Epub 2019/12/20. doi: 10.1126/scitranslmed.aax4077. PubMed PMID: 31852798.

Supporting information

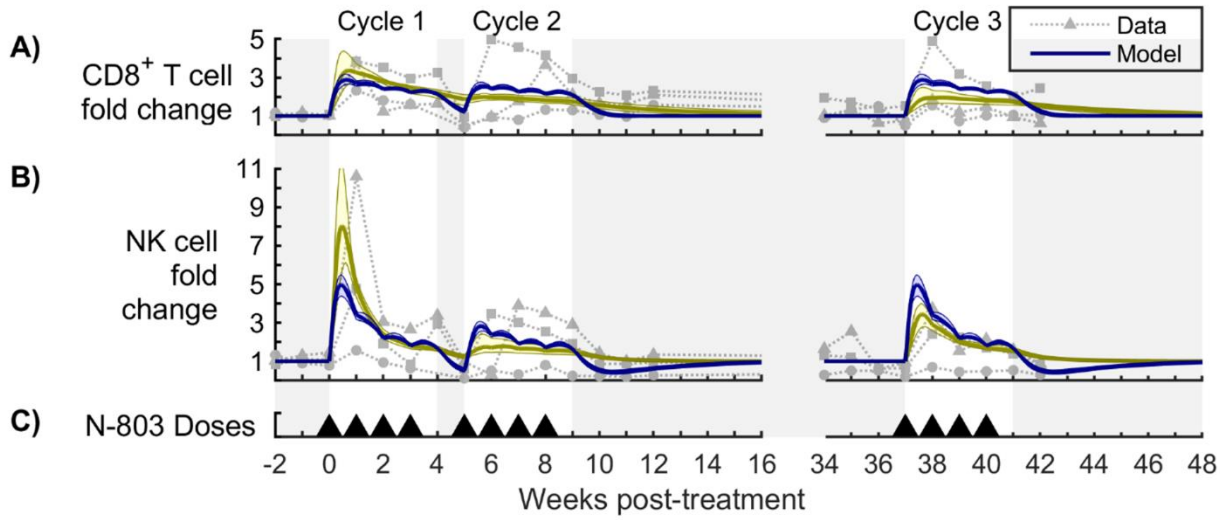

Fig S1. Model comparison with respect to cytotoxic cells, per-cell killing rate. Panels (A,B) show fold change in $CD8^+$ T cells and NK cells in the peripheral blood, respectively, for the model without immune regulation (yellow model #2) and the model without drug tolerance or viral escape (i.e. immune regulation only, blue model #4). Panel (C) shows timing of 0.1 mg/kg subcutaneous doses of N-803. Model outputs are shown as the mean (solid line) and range (shaded region) of model outputs from the top 20 parameter sets (lowest NLL) from the calibration procedure. Methodological details and fitted parameter values are given in S1 Appendix. Data from N-803-treated SIV-infected NHPs are shown as different symbols for each NHP [16].

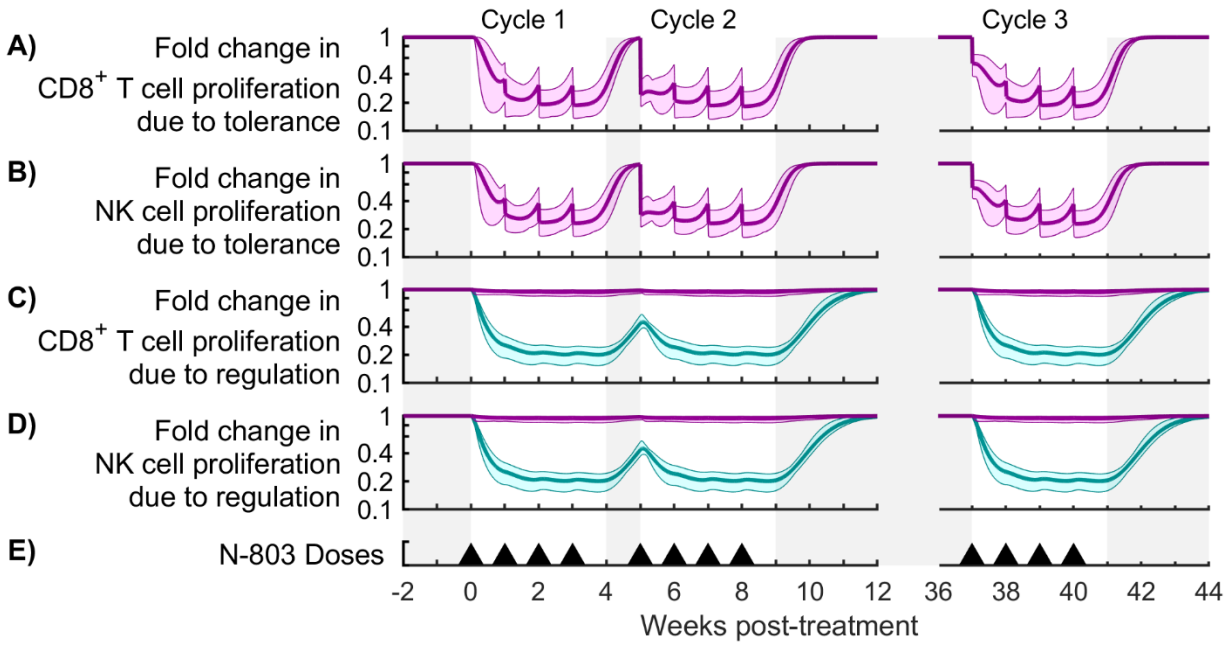

Fig S2. Contributions of drug tolerance and immune regulation to cytotoxic cell proliferation. Shown are measures of mechanism contribution to $CD8^+$ T cell and NK cell proliferation for the model with immune regulation and viral escape (cyan model #1) and the model with immune regulation and drug tolerance (purple model #3). Panels (A,B) show the fold change in $CD8^+$ T cell proliferation and NK cell proliferation due to tolerance (Eq. S19 in S1 Appendix). Panels (C,D) show the fold change in $CD8^+$ T cell proliferation and NK cell proliferation due to regulation (Eq. S18 in S1 Appendix). Panel (E) shows timing of 0.1 mg/kg subcutaneous doses of N-803. Model outputs are shown as the mean (solid line) and range (shaded region) of model outputs from the top 20 parameter sets (lowest NLL) from the calibration procedure. Methodological details and fitted parameter values are given in S1 Appendix..

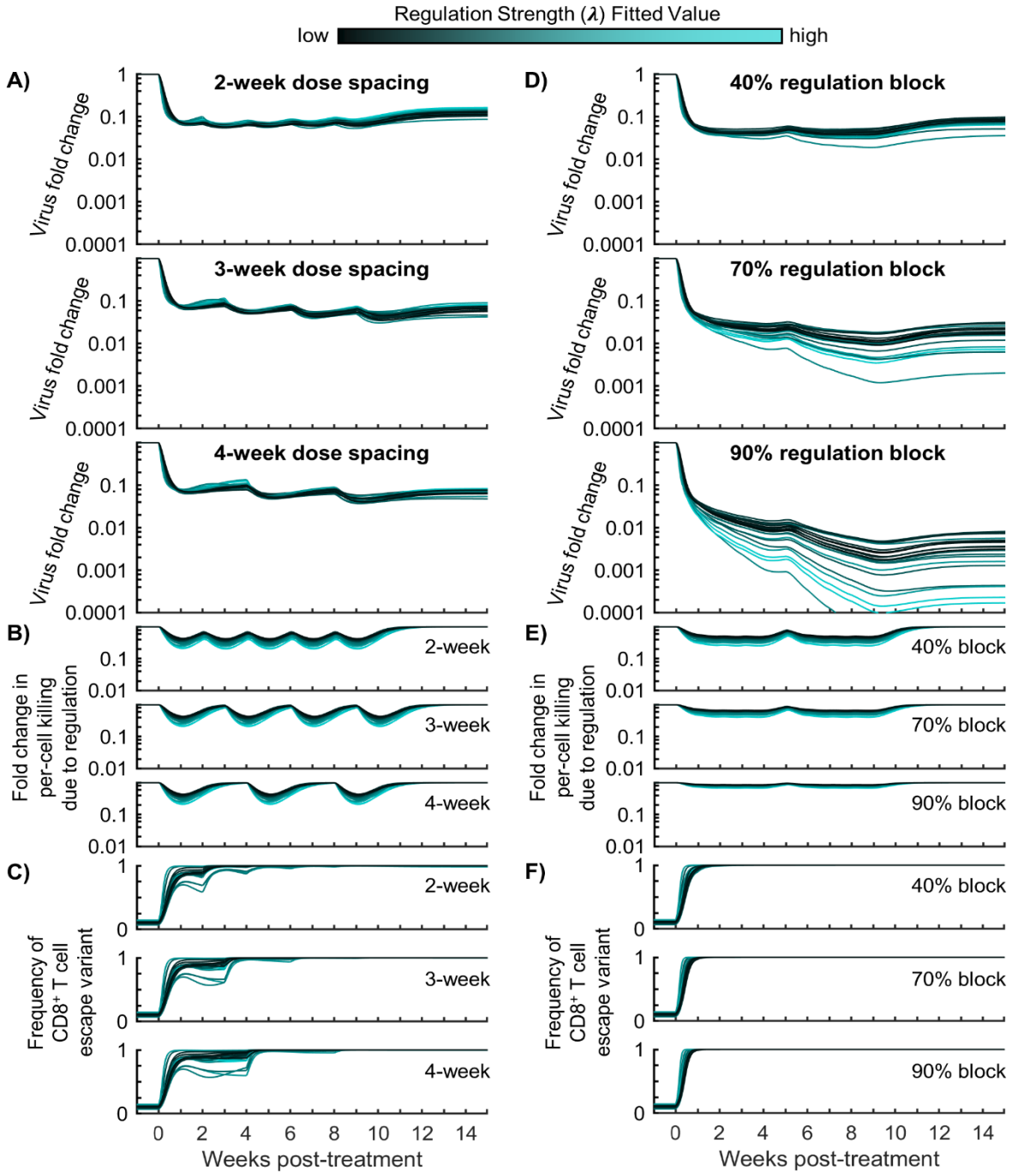

Fig S3. Time courses for N-803 regimen changes for model #1. Panels (A-C) show the results of changing the N-803 dosing frequency for the model with immune regulation and viral escape (model #1). Panel (A) shows the fold change in viral load corresponding to the 0.1 mg/kg subcutaneous dosing regimens with 2-, 3-, and 4-week dosing. Panel (B) shows the corresponding fold changes in per-cell killing due to regulation (Eq. S14). Panel (C) shows the corresponding changes in the frequency of the $CD8^+$ T cell escape variant. Panels (D-F) show the response of model #1 to the 1-week dosing regimen (Fig 2D) delivered along with regulatory blockade (simulated by 40, 70, and 90% reduction of killing regulation parameter λ). Shown are the results from the top 20 models from the calibration procedure, shaded according to the fitted value of the killing regulation strength parameter λ (before applying regulatory blockade).

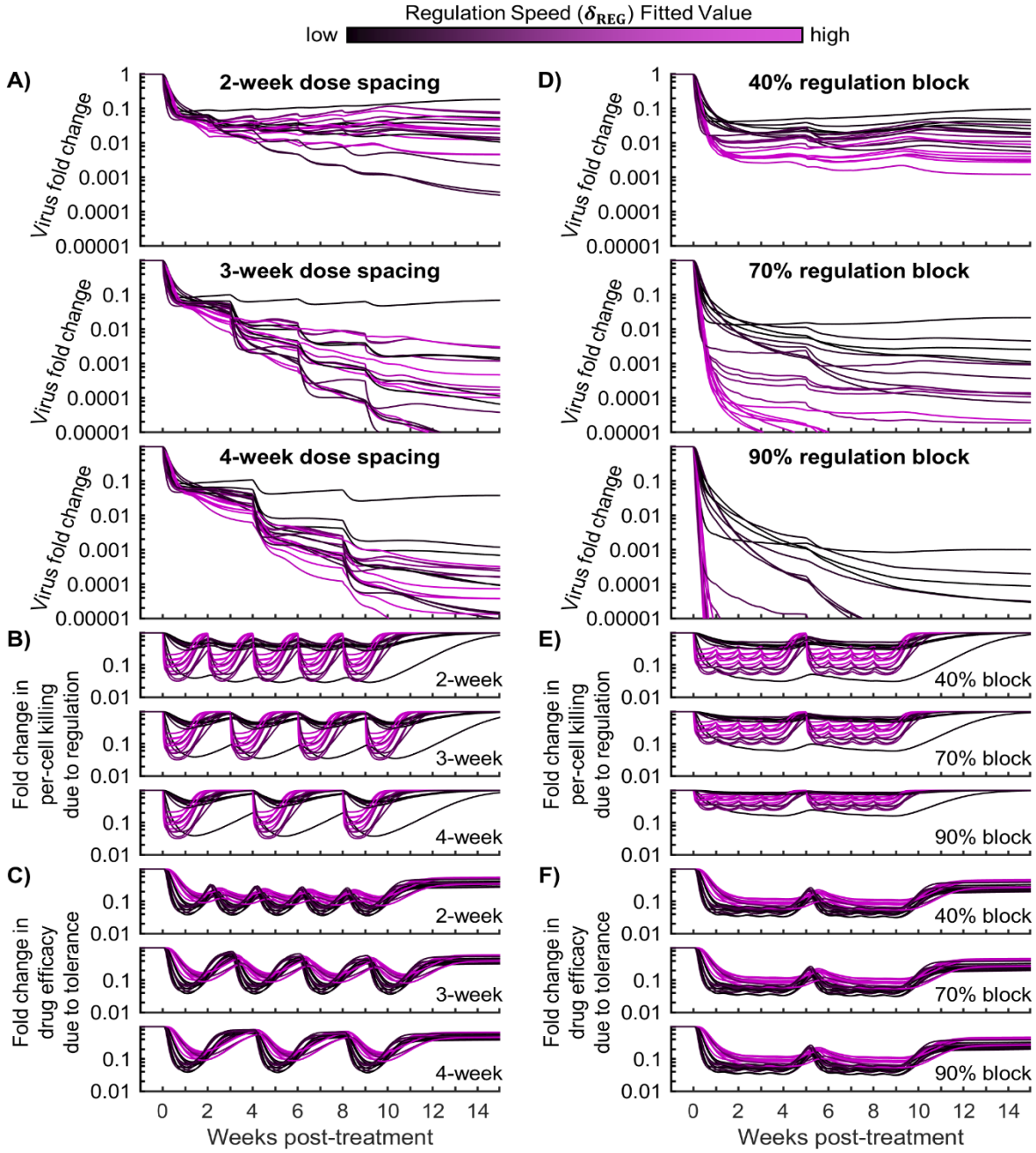

Fig S4. Time courses for N-803 regimen changes for model #3. Panels (A-C) show the results of changing the N-803 dosing frequency for the model with immune regulation and drug tolerance (model #3). Panel (A) shows the fold change in viral load corresponding to the 0.1 mg/kg subcutaneous dosing regimens with 2-, 3-, and 4-week dosing. Panel (B) shows the corresponding fold changes in per-cell killing due to regulation (Eq. S14). Panel (C) shows the corresponding fold changes in drug efficacy due to tolerance (Eq. S13). Panels (D-F) show the response of model #3 to the 1-week dosing regimen (Fig 2D) delivered along with regulatory blockade (simulated by 40, 70, and 90% reduction of killing regulation parameter λ). Shown are the results from the top 20 models from the calibration procedure, shaded according to the fitted value of the regulation speed parameter δ_{REG}.

Mathematical modeling of N-803 treatment in SIV-infected non-human primates: S1 Appendix

Supplemental Methods

Model assumptions

The following is a discussion of noteworthy assumptions in the model (Eq. 1-14 in the main text). Healthy target cells are assumed constant, which follows from two considerations. First, it was observed that total peripheral blood CD4$^+$ T cells remained approximately constant during the N-803 treatment under consideration [1]. Second, during chronic HIV infection, only about ~2% of HIV-infected cells are replication-competent [2]. Taken together, these support the assumption that the healthy CD4$^+$ T cells remained approximately constant over the time periods under consideration in this work.

A quasi-steady-state for virions relative to infected CD4$^+$ T cells was assumed. Both HIV and SIV are cleared quickly from the plasma, with a virion half-life on the order of minutes [3-5]. Therefore, any delay between changes in infected cells and changes in virions was on a much shorter timescale than the dynamics of the observed system. The quasi-steady state implies that virions are proportional to infected cells (i.e. $V=kI_V$ and $W=kI_W$) and allows Eq. (1,2) to be rewritten in terms of the free virions, V and W (Eq. S1,S2). Note that constants are defined collectively as $q_V=b_VTk-d_I$ and $q_W=b_WTk-d_I$.

$$[V]' = q_V[V] - g_E[E][V] - g_K[K][V] \tag{S1}$$

$$[W]' = q_W[W] - \chi g_E[E][W] - g_K[K][W] \tag{S2}$$

The assumptions of constant target cells and quasi-steady-state of the free virus relative to infected cells have been used together in models of HIV treatment [6, 7].

Assuming steady-state prior to treatment, some parameters were derived from Eq. (3,4,S1,S2). Specifically, proliferation rates for virus (q_V,q_W) were calculated from killing parameters (g_E,g_K,χ), and proliferation rates of cells (r_E,r_K) are calculated from cytotoxic cell parameters (d_E,d_K,h). The expressions for derived parameter values, which include initial conditions $[E](0)$ and $[K](0)$, are given in Eq. (S3-S6).

$$q_V = g_E[E](0) + g_K[K](0) \tag{S3}$$

$$q_W = \chi g_E[E](0) + g_K[K](0) \tag{S4}$$

$$r_E = d_E\left(h + [E](0)\right)/h \tag{S5}$$

$$r_K = d_K\left(h + [K](0)\right)/h \tag{S6}$$

Cell types and activation. We convolved all CD8⁺ T cells into one variable (E), and we convolved all NK cells into another variable (K). Killing rate constants (g_E,g_K) were applied to each of these total populations. Modifications to killing rate via drug stimulation, drug tolerance, and immune regulation (Eqs. 7,8) represented changes in both the frequency of cytotoxically active cells within their respective total populations and changes in the individual efficacy cytotoxically active cells. We also neglect any delay between changes in antigen-dependent memory CD8⁺ T cell activation and changes in the overall killing rate, based on multiple considerations. First, chronic infections such as SIV include persistent CD8⁺ T cell activation. Second, memory CD8⁺ T cells acquire cytotoxic effector functions within 24 hours after antigen stimulation [8, 9]. Third, IL-15 promotes bystander activation of CD8⁺ T cells [10-12]. Such cells were capable of non-specific cytotoxicity of hepatitis-A-infected cells in a manner similar to NK cells [13].

Immune regulation and drug tolerance. We employ phenomenological representations of immune regulation and drug tolerance, with the two mechanisms being distinguished by their effect and their dynamics. Immune regulation directly reduces rates of killing and proliferation for CD8⁺ T cells and NK cells (via λ,φ), while drug tolerance inhibits N-803 stimulation of these processes (via η). Both the generation and decay of the immune regulatory signal is governed by a single parameter (δ_{REG}), while drug tolerance is governed by two parameters (δ_{TOL},τ). The tolerance recovery parameter (τ) allows drug tolerance to persist across long gaps in treatment, while immune regulation cannot persist long-term. We make no assumptions as to the sources of immune regulation or drug tolerance. For example, IL-15 receptor expression (modeled by drug tolerance) can be modulated by a variety of signals. CD122 expression is increased following antigen stimulation [14-16], while IL-6 can inhibit the upregulation of CD122 in follicular helper T cells [17]. IL-15 increased CD122 expression in memory CD8⁺ T cells of NHPs [18]. In our data, a transient increase in CD122 was also observed in effector memory CD8⁺ T cells during the first few weeks of treatment [1]. The effect of native cytokine signaling, including IL-15, is convolved into rate constants (e.g. g_E,g_K,d_E,d_K). We also convolve the effect of receptor levels on native cytokine activity into drug stimulation, immune regulation, and drug tolerance terms (Eq. 7-8).

Model calibration

The model described by Eq. (3-14,S1-S6) was simultaneously calibrated to plasma viral load, $CD8^+$ T cell peripheral blood count, and NK cell peripheral blood count measured in three rhesus macaques chronically infected with SIV and given an N-803 regimen (Fig 2) [1]. We calibrated the model using a multi-start local search approach implemented in MATLAB version R2018b (Mathworks). The parameter space was sampled on a logarithmic scale via Latin hypercube sampling [19] using the MATLAB 'lhsdesign' function (3600 samples). Each sample set of parameter values was used as an initial guess in an interior-point optimization algorithm [20] implemented by the MATLAB 'fmincon' function. This algorithm, also operating on the logarithmic parameter values, returned a local minimum of the negative loglikelihood (NLL) with respect to the log-fold change in virus, fold change in $CD8^+$ T cells, and fold change in NK cells in all three subjects. Some viral data points lay on the lower limit of detection for the viral assay. For these points, error was only counted if the model value was above the data point. Once the NLL had been minimized from each sample parameter set, the results were ranked to find the parameter set corresponding the global minimum NLL. The parameter distributions corresponding to the top 5% of models were used to narrow the parameters space, and the entire calibration process was repeated twice more (i.e. three total iterations of the parameter space). The mean and range of the outputs from the top 20 (top 1% or less) of fitted parameter sets were considered when discussing the model.

Parameter space

A subset of parameters with sufficient experimental support was fixed during calibration (Table S1) to improve the identifiability of the remaining parameters. For example, pharmacokinetic parameters were fixed at experimental estimates to allow the N-803 50% effective concentration (C_{50}) to be identified [21, 22]. We used non-human primate data whenever available. Parameters that were not fixed were restricted within biologically feasible ranges, if available (Table S2). Some parameters, such as regulation strength (λ,φ) and tolerance strength (η), had no measurable experimental analog. Ranges for these parameters were intentionally broad, allowing the calibration process to determine the necessary values.

The following is a discussion of the fixed parameters in Table S1. Initial conditions for SIV plasma viral load, $CD8^+$ T cells, and NK cells, where the respective means of pre-treatment data across all 3 subjects (15 samples total for each species) [1]. Initial N-803 at the absorption site was based on measured N-803 molecular weight of 114 kDa [23] and the administered dose of 0.1 mg/kg

[1]. The N-803 absorption rate constant (k_a) was obtained from the elimination phase of the plasma pharmacokinetics following a 10 μg/kg subcutaneous dose in humans participating in cancer trials [22]. N-803 clearance rate constant (k_e) was obtained from the half-life (7.97 ± 1.29 h) reported following a 0.1 mg/kg intravenous dose in cynomolgus macaques [21]. The ratio of the N-803 volume of distribution and bioavailability (v_d/F) was obtained from the volume of distribution (37.56 ± 9.1 mL/kg) reported for a 0.1 mg/kg intravenous dose in cynomolgus macaques [21] and the bioavailability (0.0299 ± 0.0160) reported for a 10 μg/kg subcutaneous dose in humans [22]. The number of tolerance variables (N) and number of regulation variables (M) were chosen to reflect dynamics of N-803 receptors CD122 and CD132 and inhibitory markers CD39 and PD-1, respectively, on $CD8^+$ T cells and NK cells [1]. The number of tolerance variables (N) was higher to reflect the delay in receptor changes with respect to inhibitory marker changes.

The following is a discussion of the varied parameters in Table S2. The N-803 50% effect concentration (C_{50}) was based on the ex vivo 50% effect concentration for $CD8^+$ T cells and NK cells in rhesus macaques (estimated as 10-1000 pM from figure) [24]. The lower limit was then adjusted to account for the possibility of higher concentrations of N-803 in the lymph tissue relative to the blood, as evidenced by murine tissue biodistribution data [21]. The $CD8^+$ T cell killing rate constant (g_E) was based on the range of estimates of total HIV-infected cell death rate due to $CD8^+$ T cells (reviewed in [25]) and peripheral blood concentration of ~500 $CD8^+$ T cells per μL (used as initial condition). NK cell killing rate constant (g_K) was assumed to be some fraction of $CD8^+$ T cell killing rate based on comparison of viral load after CD8 depletion (elimination of $CD8^+$ T cells and NK cells) [26] and CD16 depletion (elimination of NK cell cytotoxic subgroup) [27]. The cell death rate constants (d_E, d_K) were based on $CD8^+$ T cell and NK cell turnover in SIV-infected rhesus macaques [28]. The upper limits were increased to fit the rate of contraction following N-803 observed in the NHP data [1]. Thus, the value incorporates changes in survival signals due to N-803 treatment and immune regulation. Proliferation stimulation factors (ρ_E, ρ_K) were limited according to maximum allowed expansion rates ($\rho_E \cdot d_E$, $\rho_K \cdot d_K$). These rates were derived from Eq. (3-4,7-8) by assuming h >> $[E]$,$[K]$. The maximum expansion rates are limited based on $CD8^+$ T cell clonal expansion rate for rhesus macaques (~1/day) [29].

Table S1. Model parameters fixed during calibration.

Parameter	Symbol	Value	Units	Reference
Initial SIV virions in plasma (both variants) [a]	$[V](0)+[W](0)$	3.83	log(CEQ/ml)	[1]
Initial CD8⁺ T cells in peripheral blood	$[E](0)$	520	#/μL	[1]
Initial NK cells in peripheral blood	$[K](0)$	231	#/μL	[1]
Initial N-803 at absorption site	$[X](0)$	880	pmol/kg	[23]
N-803 absorption rate constant	k_a	0.80	/day	[22]
N-803 clearance rate constant	k_e	2.1	/day	[21]
N-803 volume of distribution / bioavailability	v_d/F	1.3	L/kg	[21, 22]
Number of tolerance variables	N	6		[1]
Number of regulation variables	M	2		[1]

Initial conditions, pharmacokinetic parameters (Eq. 5-6), and the number of tolerance and regulation variables (Eq. 10-12,14) were held fixed at the given values during all analysis.

[a] We assume SIVmac239 gag copy equivalents in the plasma to be proportional to SIV virions in the peripheral blood. The initial conditions for the virus variants V and W were determined from the total initial viral load (Table S1) and the initial frequency of variant W (Table S2).

Table S2. Model parameters varied during calibration.

Parameter	Symbol	Range	Units	Reference
N-803 50% effective concentration	C_{50}	(1, 1000)	pM	[21, 24]
Tolerance rate constant	δ_{TOL}	(0.05, 5)	/day	
Regulation rate constant	δ_{REG}	(0.05, 5)	/day	
Tolerance recovery	τ	(0.001, 1)		
Escape variant initial frequency [a]	f	(0.001, 1)		
Escape variant susceptibility factor	χ	(0.001, 1)		
CD8⁺ T cell death rate constant	d_E	(0.01, 1)	/day	[28]
NK cell death rate constant	d_K	(0.01, 1)	/day	[28]
CD8⁺ T cell killing rate constant	g_E	($2\cdot10^{-5}$, 0.02)	μL/#·d	[25]
NK cell / CD8⁺ T cell killing rate ratio [b]	g_K/g_E	(0.01, 1)		[26, 27]
Maximum proliferating cells	h	(20, 2000)	#/μL	
CD8⁺ T cell maximum expansion rate [c]	$\rho_E \cdot d_E$	(0.02, 2)	/day	[29]
NK cell maximum expansion rate [c]	$\rho_K \cdot d_K$	(0.02, 2)	/day	[29]
CD8⁺ T cell killing stimulation factor	γ_E	(0.01, 100)		
NK cell killing stimulation factor	γ_K	(0.01, 100)		
Tolerance effect factor	η	(0.01, 100)		
Proliferation regulation factor	φ	(0.01, 100)		
Killing regulation factor	λ	(0.01, 100)		

Shown are the allowed ranges for parameter values during calibration and model comparison. Parameters were sampled logarithmically from the given ranges.

[a] The initial conditions for the virus variants V and W were determined from the total initial viral load (Table S1) and the initial frequency of variant W (Table S2).

[b] The value of the NK cell killing rate constant g_K is defined as some fraction of CD8⁺ T cell killing rate constant g_E.

[c] The value of proliferation stimulation factors ρ_E, ρ_K are defined by the maximum expansion rates of their respective populations.

Model comparison

Model comparison was used to identify which model mechanisms (drug tolerance, immune regulation, or viral escape) were required to reproduce the dynamics observed in N-803-treated NHPs. Calibration was performed for the full model (Eq. 3-14,S1-S6) as well as for four additional models (Table S3). Three of the models had either 1) drug tolerance, 2) immune regulation, or 3) viral escape removed. Thus, each of these models combined two of the three mechanisms. The fourth model included only immune regulation (no drug tolerance or viral escape).

Models were compared based on their quantitative and qualitative ability to reproduce the experimental results. The quantitative assessment was done by comparing both the negative log-likelihood and the Akaike Information Criterion (Eq. S7) [30].

$$\mathrm{AICc} = 2\times \mathrm{NLL} + 2P + \frac{2P\left(P+1\right)}{S-P-1} \tag{S7}$$

This criterion includes the negative log-likelihood, NLL. It is also penalized by the number of model parameters, P (Table S3), and corrected for the number of data points, S = 289.

Qualitative assessment was based on the ability of each model to reproduce key features of the measured viral load dynamics [1]. This assessment focused on the viral load, as it is the most relevant treatment outcome. Three qualitative criteria were employed based on the response of the virus to each of the three treatment cycles. For the first treatment cycle (weeks 0-4), the viral load was observed to drop sharply during the first 1-2 weeks, followed by a partial rebound that began by week 3. For the second treatment cycle (weeks 5-9), the viral load had a negligible response. For the third treatment cycle (weeks 37-41), the viral load had a response similar to, yet lesser than, that of the first cycle. Both quantitative and qualitative criteria were considered together to predict how each mechanism contributed to observed viral dynamics during treatment.

Table S3. Summary of models compared.

	Drug Tolerance	Immune Regulation	Viral Escape	Parameters Removed	Number of Parameters
Control	√	√	√	none	27
Model #1		√	√	N, δ_{TOL}, τ, η	23
Model #2	√		√	M, δ_{REG}, φ, λ	23
Model #3	√	√		f, χ	25
Model #4		√		N, δ_{TOL}, τ, η, f, χ	21

Variant models #1-#4 were created by fixing select parameters at zero in Eq. (3-14,S1-S6).

Per-cell cytotoxicity (PCK) and related equations

In order to quantify the effect of immune regulation, drug tolerance, and viral escape on per-cell cytotoxic activity, we defined per-cell killing (PCK). The following is a derivation of the expression for per-cell killing (PCK). To begin, the rates of change for each viral variant (Eq. S1,S2) can be added together to describe the rate of change of the total virus (Eq. S8).

$$[V]' + [W]' = q_V [V] + q_W [W] - g_E [E]([V] + \chi [W]) - g_K [K]([V] + [W]) \quad \text{(S8)}$$

We next introduce v, w, e, k as frequencies of virus or killer cells within their respective groups (e.g. $[v]=[V]/([V]+[W])$ or $[e]=[E]/([E]+[K])$). Collecting terms in Eq. (S8) results in an expression that is similar in form to Eq. (S1,S2) but applies to the sum of $CD8^+$ T cells and NK cells and the sum of both viral variants.

$$[V+W]' = \left(q_V [v] + q_W [w]\right)[V+W] - \left\{\left([v] + \chi [w]\right) g_E [e] - g_K [k]\right\}[E+K][V+W] \quad \text{(S9)}$$

There is a collection of terms that behaves the same way as killing rate constants (g_E,g_K) in Eq. (S1,S2). This expression is the per-cell killing (PCK) absent N-803 intervention (Eq. S10).

$$\text{PCK} = \frac{[\text{total killing rate}]}{[\text{killer cells}][\text{virus}]} = \left([v] + \chi [w]\right) g_E [e] - g_K [k] \quad \text{(S10)}$$

Supplementing this with changes in killing rate due to N-803 stimulation, drug tolerance, and immune regulation (Eq. 7 in main text) results in the expression for PCK during N-803 treatment (Eq. S11-S13).

$$\text{PCK} = \frac{[\text{total killing rate}]}{[\text{killer cells}][\text{virus}]} = \frac{([v] + \chi[w]) g_E \left(1 + \gamma_E [\Theta][\Omega]\right)[e] + g_K \left(1 + \gamma_K [\Theta][\Omega]\right)[k]}{1 + \lambda [\text{REG}_M]} \quad \text{(S11)}$$

$$[\Theta] = \left(\frac{[C]}{C_{50} + [C]}\right) \quad \text{(S12)}$$

$$[\Omega] = \left(\frac{1}{1 + \eta\left([\text{TOL}_{N-1}] + [\text{TOL}_N]\right)}\right) \quad \text{(S13)}$$

The effects of immune regulation, drug tolerance, and viral escape on PCK were calculated as follows (Eq. S14-S16). The fold change in PCK due to one mechanism was quantified as the ratio of per-cell killing (PCK) with that mechanism to the PCK without that mechanism.

Immune regulation:

$$\frac{\text{PCK}}{\text{PCK}(\lambda=0)} = \frac{1}{1 + \lambda [\text{REG}_M]} \quad \text{(S14)}$$

Drug tolerance:

$$\frac{\text{PCK}}{\text{PCK}(\eta=0)} = \frac{([v]+\chi[w])g_E\left(1+\gamma_E[\Theta][\Omega]\right)[e]+g_K\left(1+\gamma_K[\Theta][\Omega]\right)[k]}{([v]+\chi[w])g_E\left(1+\gamma_E[\Theta]\right)[e]+g_K\left(1+\gamma_K[\Theta]\right)[k]} \tag{S15}$$

Viral escape:

$$\frac{\text{PCK}}{\text{PCK}(\chi=1)} = \frac{([v]+\chi[w])g_E\left(1+\gamma_E[\Theta][\Omega]\right)[e]+g_K\left(1+\gamma_K[\Theta][\Omega]\right)[k]}{g_E\left(1+\gamma_E[\Theta][\Omega]\right)[e]+g_K\left(1+\gamma_K[\Theta][\Omega]\right)[k]} \tag{S16}$$

We introduced a measure of viral fitness by calculating the fold change in the overall viral proliferation rate during treatment (Eq. S17).

$$\begin{bmatrix}\text{fold change in}\\ \text{viral fitness}\end{bmatrix} \propto \begin{bmatrix}\text{fold change in}\\ \text{viral proliferation}\end{bmatrix} = \frac{q_V[v]+q_W[w]}{q_V(1-f)+q_W f} \tag{S17}$$

Fold change in $CD8^+$ T cell and NK cell proliferation due to immune regulation and drug tolerance (Fig S2) were calculated in a manner similar to fold changes in per-cell killing due to immune regulation and drug tolerance (from Eq. 8 in the main text). For example, the fold change in $CD8^+$ T cell proliferation due to immune regulation (Eq. S18) is defined by the ratio of the proliferation rate with immune regulation over the proliferation rate without immune regulation ($\varphi = 0$).

Immune regulation:

$$\frac{\text{Proliferation}}{\text{Proliferation}(\varphi=0)} = \frac{1}{1+\varphi\left[\text{REG}_M\right]} \tag{S18}$$

Drug tolerance:

$$\frac{\text{Proliferation}}{\text{Proliferation}(\eta=0)} = \frac{1+\rho_i[\Theta][\Omega]}{1+\rho_i[\Theta]} \quad i=E,K \tag{S19}$$

Significance testing

Statistical comparison of the results of treatment exploration (Fig 7) was conducted in GraphPad Prism 8. Separate analyses were conducted for changes due to dose spacing (Fig 7A) and for changes due to regulation blockade (Fig 7B), but the same technique was used. For example, this was a two-way ANOVA incorporating the model (#1 vs #3) and the dose spacing (1-4 weeks). Data points were matched by model parameter set, employing the Geisser-Greenhouse correction for non-sphericity. Thus, we treated the results from each parameter set (20 sets for each model) as though they had come from the same subject in a longitudinal study. The Tukey test for multiple comparisons was conducted to test the statistical significance of the difference of means between each dose spacing.

Sensitivity analysis

A sensitivity analysis was conducted to quantify the correlations between model parameters and the treatment efficacy over multiple timescales in the full model. As a measure of treatment efficacy, we considered the drop in viral load for each treatment cycle (Fig S5). This was defined as the difference between the viral load at the start of the cycle (e.g. viral load at week 0) and the minimum viral load across that cycle (e.g. minimum viral load between week 0 and week 4). We used partial rank correlation coefficients (PRCC) calculated via the MATLAB 'partialcorr' function [31]. A Latin hypercube sample of 10,000 parameter sets was generated from a wide parameter space (Table S4). The model was evaluated at each parameter set, and PRCC were calculated between each parameter and the viral load drop for each of the three treatment cycles. Correlations that were significant at α=0.0001 across three repetitions of 10,000 samples were considered valid.

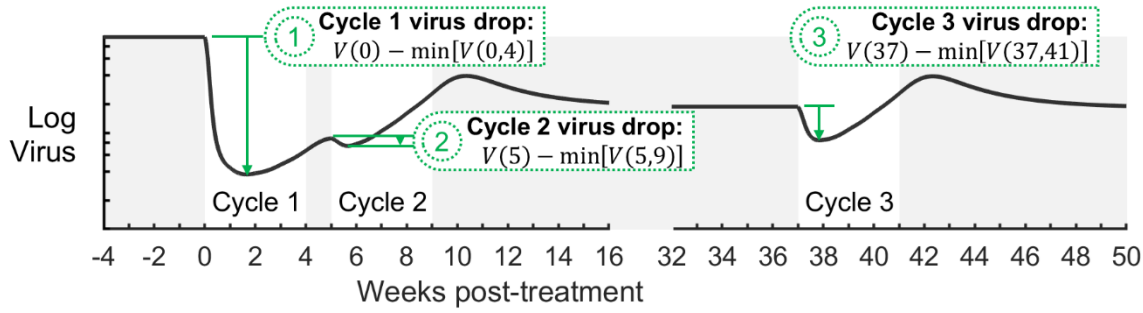

Fig S5. Metrics for N-803 treatment efficacy considered during sensitivity analysis. The drop in viral load during each treatment cycle (1,2,3) was used as a measure of treatment efficacy. The viral load drop is defined as the difference between the viral load at the start of the cycle (e.g. viral load at week 0) and the minimum viral load across that cycle (e.g. minimum viral load between week 0 and week 4). Each metric is highlighted using a representative viral trajectory.

Table S4. Model parameters varied during sensitivity analysis.

Parameter	Symbol	Range	Units
N-803 50% effect concentration	C_{50}	(0.4, 40)	pM
Tolerance rate constant	δ_{TOL}	(0.05, 5)	/day
Regulation rate constant	δ_{REG}	(0.05, 5)	/day
Tolerance recovery	τ	(0.001,1)	
Escape variant initial frequency	f	(0.001, 1)	
Escape variant susceptibility factor	χ	(0.001, 1)	
CD8⁺ T cell death rate constant	d_E	(0.01, 1)	/day
NK cell death rate constant	d_K	(0.01, 1)	/day
CD8⁺ T cell killing rate constant	g_E	(10^{-5}, 0.01)	μL/#·d
NK cell killing rate constant	g_K	(10^{-5}, 0.01)	μL/#·d
Maximum proliferating cells	h	(50, 5000)	#/μL
CD8⁺ T cell proliferation stimulation factor	ρ_E	(0.1, 10)	
NK cell proliferation stimulation factor	ρ_K	(0.1, 10)	
CD8⁺ T cell killing stimulation factor	γ_E	(0.01, 100)	
NK cell killing stimulation factor	γ_K	(0.01, 100)	
Tolerance effect factor	η	(0.01, 100)	
Proliferation regulation factor	φ	(0.1, 10)	
Killing regulation factor	λ	(0.01, 100)	

Shown are the allowed ranges for parameter values during sensitivity analysis. Parameters were sampled logarithmically from the given ranges via Latin hypercube sampling [19]. Parameters not shown were fixed (Table S1).

Supplemental Results

Discussion of sensitivity analysis

To assess the relative impact of each treatment response mechanism on viral responses, we performed global sensitivity analysis. This analysis correlates changes in parameter values to changes in model outputs in the context of other parameter influences. We calculated the partial rank correlations coefficients (PRCCs) (Table S5) between model parameters and model outputs of interest. The parameters of interest are those governing drug tolerance, immune regulation, and viral escape. The outputs of interest are the viral load drop during each treatment cycle which we use as a metric of treatment efficacy in each cycle (Fig S5).

Parameters governing immune regulation had strong correlations with treatment efficacy. Strong killing regulation (i.e. high λ) is associated with low efficacy (small viral drop) in all three cycles, having the strongest impact in cycle 1. Strong proliferation regulation (i.e. high φ) correlates with lower efficacy (smaller viral drop) in cycle 2, reflecting the delay that comes from acting on viral load indirectly through suppressing CD8⁺ T cell and NK cell population expansion. A fast

regulatory response (i.e. high δ_{REG}) correlated with lower efficacy (smaller viral drop) in cycle 1 and cycle 3. In contrast, fast regulatory response was also associated with higher efficacy in cycle 2, which follows a shorter 2-week break in treatment. Recall that high δ_{REG} also causes regulation to abate quickly after treatment. Taken together, these correlations indicate that: 1) successive doses are more effective if they are timed such that the regulatory signal is allowed to abate between doses; and 2) directly blocking regulation (e.g. lowering λ or φ) could improve treatment response to N-803.

Correlations between tolerance parameters and treatment efficacy mirrored those of regulation, with some key differences. Tolerance strength (η) had correlations that fell between those of killing regulation strength (λ) and proliferation regulation strength (φ). This reflects how tolerance strength (η) reduces N-803 stimulation of both cytotoxicity and proliferation of $CD8^+$ T cells and NK cells. Rapid onset of tolerance (i.e. high δ_{TOL}) was also correlated with lower treatment efficacy in cycle 1. Unlike regulation speed (δ_{REG}), the direction of the correlation for tolerance speed did not change for cycle 2. Based on the NHP data, the drug tolerance model mechanism was structurally slower than regulation based on the number of delay variables (N = 6 for tolerance and M = 2 for regulation). With tolerance being slower to adapt, the 2-week break between cycles 1 and 2 was too short to allow the effects of tolerance to subside. However, the tolerance recovery parameter (τ) had a comparably positive correlation to the treatment effectiveness in cycle 3 as regulation speed had to cycle 2. Together, this reflects how tolerance and regulation effects of previous treatment cycles may alter the outcome of the subsequent treatment cycles.

High initial frequency of the escape variant (i.e. high f) is correlated with lower treatment efficacy in cycle 1 but not cycle 2. This difference between cycles 1 and 2 is because the escape variant (W) largely replaced the dominant variant (V) due to the selective pressure of treatment in cycle 1. The correlation reappears in cycle 3, as the original dominant variant recovers in the break between cycles 2 and 3 due to a fitness advantage over the escape variant. High susceptibility of the escape variant to $CD8^+$ T cells (i.e. high χ) was associated with higher treatment efficacy in all three treatment cycles. This consistent correlation across cycles is indicative of how viral escape, as modeled here, leads to persistent loss of efficacy.

Table S5. Sensitivity analysis.

Measure of treatment efficacy	Killing Regulation Strength	Proliferation Regulation Strength	Regulation Speed	Tolerance Strength	Tolerance Speed	Tolerance Recovery	Variant W Initial Frequency	Variant W Susceptibility to T cells	Dummy Variable
	λ	ϕ	δ_{REG}	H	δ_{TOL}	τ	f	χ	
Cycle 1 virus drop	**−0.60**	**−0.13**	**−0.50**	**−0.21**	**−0.23**	-	**−0.30**	**+0.25**	-
Cycle 2 virus drop	**−0.49**	**−0.36**	**+0.07**	**−0.47**	**−0.07**	-	-	**+0.13**	-
Cycle 3 virus drop	**−0.35**	**−0.08**	**−0.39**	**−0.17**	**−0.07**	**+0.07**	**−0.06**	**+0.23**	-

Shown are the partial rank correlation coefficients (PRCC) of select model parameters to N-803 treatment efficacy, as measured by the drop in viral load during each cycle (Fig S5). The strongest possible negative correlation is −1, and the strongest possible positive correlation is +1. Correlations shown had p-value <= 0.00001 across three repetitions of 10,000 samples

Comparison to IL-15 receptors and inhibitory markers

While the cytotoxicity of $CD8^+$ T cells and NK cells were modulated by multiple mechanisms, only one mechanism (immune regulation or drug tolerance) was required to account for the contraction of $CD8^+$ T cell and NK cell populations during cycle 1 (Fig S2). When drug tolerance was structurally absent (model #1), immune regulation reduced $CD8^+$ T cell and NK cell proliferation by 75-84%. When both immune regulation and drug tolerance were present (model #3), drug tolerance reduced $CD8^+$ T cell and NK cell proliferation by 72-86%, while immune regulation had a negligible effect on proliferation. The calibrated timing of regulation for model #3 was inversely correlated with that of drug tolerance (Fig S6). The cases that predicted regulation responses to be faster than tolerance responses were more consistent with the NHP data (Fig S6), where increases in the expression of inhibitory markers (PD-1 and CD39) preceded decreases in the expression of IL-15 receptors (CD122 & CD132). Taken together, these results suggest that decreases in cytotoxicity following N-803 treatment occur on a faster timescale and is mainly driven by immune regulation. In contrast, the contraction of $CD8^+$ T cell and NK cell populations occurs on a slower timescale and is mainly driven by tolerance mechanisms.

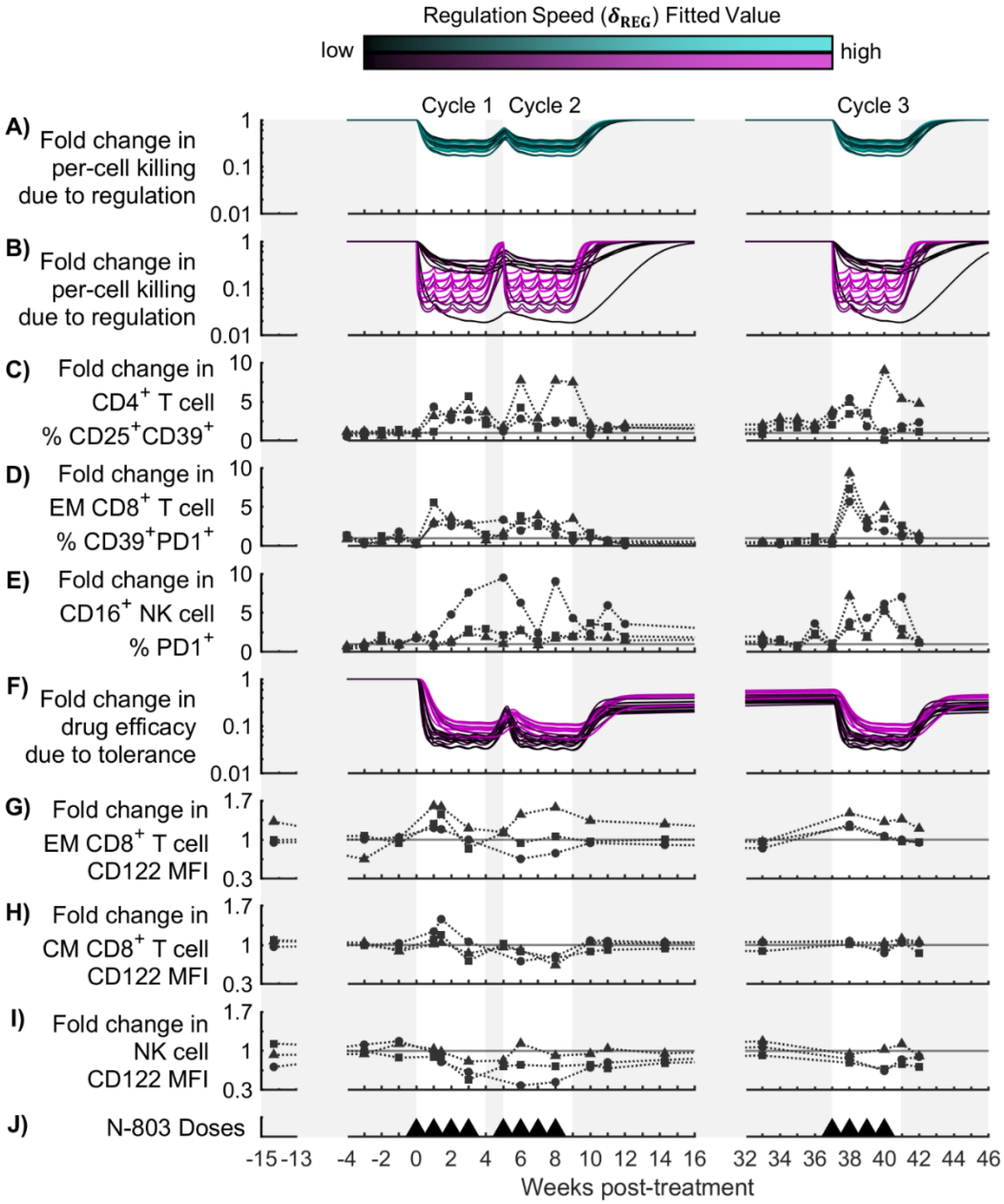

Fig S6. Comparison of regulation dynamics in model and data. Panels (A,B) show the effect of immune regulation on PCK (Eq. S14) in model #1 (immune regulation and viral escape) and model #3 (immune regulation and drug tolerance), respectively. Panel (F) shows the effect of tolerance on drug efficacy (Eq. S13) in model #3. Shown are the results from the top 20 models from the calibration procedure, shaded according to the fitted value of the regulation speed parameter δ_{REG}. Panels (C-E) and (G-H) show changes in the expression of inhibitory markers and IL-15 receptor subunits, respectively, collected along with calibration data (selected from [1]). Panel (C) shows changes in the frequency of $CD25^{+}CD39^{+}$ cells among $CD4^{+}$ T cells (i.e. regulatory T cells). Panel (D) shows changes in the frequency of $CD39^{+}PD1^{+}$ cells among effector memory $CD8^{+}$ T cells. Panel (E) shows changes in the frequency of $PD1^{+}$ cells among $CD16^{+}$ NK cells. Panels (G-I) show changes in the expression of the IL-15 receptor subunit (CD122) on effector memory $CD8^{+}$ T cells, central memory $CD8^{+}$ T cells, and NK cells. For each NHP, data is normalized to the mean of pre-treatment data points.

Model with long-term immune regulation

It is concievable that N-803 induced deviations in immune regulatory signals could persist across the long treatment gap, which could provide a simpler explanation of long-term CD8$^+$ T cell, NK cell, and SIV dynamics. To this end, a model with long-term regulation, and no drug tolerance, was also calibrated to the NHP data. This model deviates from the full model (Eq. 3-14,S1-S6.) by replacing Eq. (7,8) with Eq. (S20,S21).

$$g_i \to g_i \left[1 + \overbrace{\gamma_i \left(\frac{[C]}{C_{50} + [C]} \right)}^{\text{Drug Effect}} \right] \overbrace{\left(\frac{1}{1 + \lambda \left([\text{TOL}_{N-1}] + [\text{TOL}_N] \right)} \right)}^{\text{Immune Regulation}} \quad i = E, K \tag{S20}$$

$$r_i \to r_i \left[1 + \rho_i \left(\frac{[C]}{C_{50} + [C]} \right) \right] \left(\frac{1}{1 + \varphi \left([\text{TOL}_{N-1}] + [\text{TOL}_N] \right)} \right) \quad i = E, K \tag{S21}$$

While the model was able to reproduce the dynamics of CD8+ T cells and NK cells (Fig S7B,C), the dynamics of SIV was poorly represented (Fig S7A). The viremia decayed to a setpoint during treatment cycle 1 without the subsequent rebound observed in the NHP data. Thus, allowing immune regulation to persist long-term, absent drug tolerance, does not qualitatively match the viral dynamics.

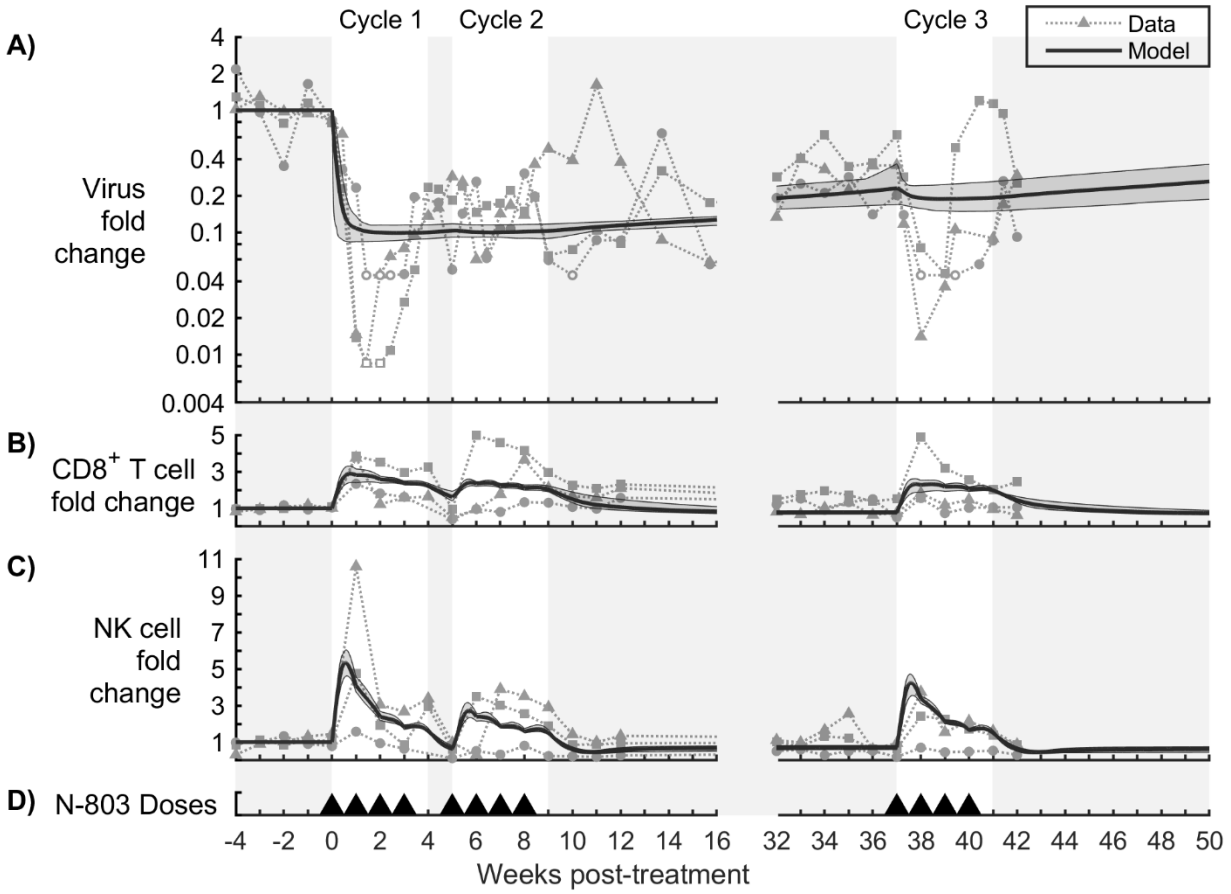

Fig S7. Long-term regulation model calibration. A model with long-term regulation, and no drug tolerance (see Eq. S20,S21), was calibrated to (A) fold change in virus in the plasma, (B) fold change in $CD8^+$ T cells in the peripheral blood, and (C) fold change in NK cells in the peripheral blood. Panel (D) shows timing of 0.1 mg/kg subcutaneous doses of N-803. Model outputs are shown as the mean (solid line) and range (shaded region) of model outputs from the top 20 parameter sets (lowest NLL) from the calibration procedure. Methodological details and fitted parameter values are given in S1 Appendix. Data from N-803-treated SIV-infected NHPs are shown as different symbols for each NHP [1]. Open symbols represent viral load below the detection limit of the assay (100 viral RNA copies/mL).

Fitted parameter values

The top 20 calibrated parameter sets (i.e. lowest NLL) were used in interpresting results for the full model (Eq. 3-14,S1-S6.) and for each additional model #1-4 (Table S3). The distributions of these parameter values are graphically summarized (Fig S8) and tabulated (Tables S6-S15).

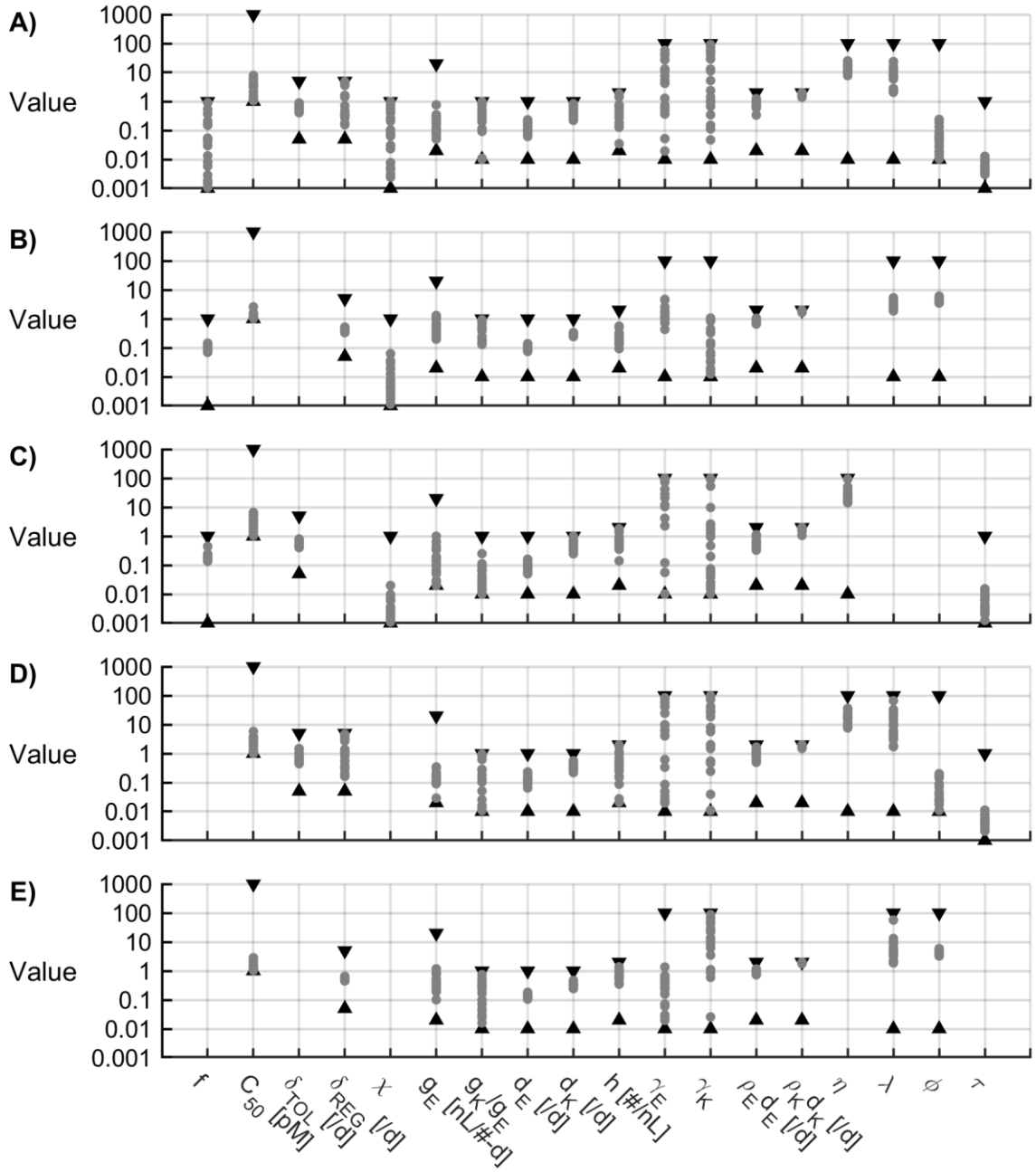

Fig S8. Calibrated parameter summary. Panel (A) summarizes the fitted parameters for the full model (Fig 2). Panels (B-D) summarize the fitted parameters for models #1-4, respectively (Figs 3,4).Triangles represent the allowed parameter range (Table S2). Dots represent the parameter values for the top 20 fitted parameter sets (i.e. 20 lowest NLL). Values are given in Tables S6-S15.

Table S6. Fitted parameters for full model (1-10 lowest NLL)

Parameter [a]		Units	#1	#2	#3	#4	#5	#6	#7	#8	#9	#10
N-803 50% effect concentration	C_{50}	pM	1.066	2.099	1.659	1.229	3.677	3.725	7.915	3.922	3.907	3.138
Tolerance rate constant	δ_{TOL}	/day	0.566	0.798	0.472	0.578	0.692	0.507	0.770	0.497	0.553	0.889
Regulation rate constant	δ_{REG}	/day	1.441	0.361	4.252	4.019	0.336	4.732	0.468	4.681	4.810	0.381
Tolerance recovery **(x 10^3)**	τ		8.289	5.469	5.970	5.758	6.371	8.158	4.481	9.779	5.992	5.057
Escape variant initial frequency **(x 10^3)**	f		536.128	29.812	199.609	5.819	54.365	13.330	48.333	51.966	2.875	368.996
Escape variant susceptibility factor **(x 10^3)**	χ		7.707	264.936	2.418	104.540	561.301	473.594	3.050	409.035	23.290	988.748
$CD8^+$ T cell death rate constant	d_E	/day	0.081	0.219	0.065	0.141	0.128	0.162	0.178	0.139	0.139	0.100
NK cell death rate constant	d_K	/day	0.366	0.674	0.836	0.400	0.424	0.618	0.490	0.348	0.309	0.541
$CD8^+$ T cell killing rate constant **(x 10^3)**	g_E	μL/#·d	0.119	0.300	0.350	0.242	0.077	0.195	0.050	0.166	0.280	0.096
NK cell / $CD8^+$ T cell killing rate ratio	g_K/g_E		0.951	0.093	0.792	0.010	0.947	0.289	0.757	0.891	0.011	0.114
Maximum proliferating cells	h	#/μL	281.450	1872.222	1423.468	464.200	653.975	665.322	1851.401	149.122	294.320	1475.726
$CD8^+$ T cell maximum expansion rate	$\rho_E \cdot d_E$	/day	0.644	0.879	0.342	0.778	0.845	0.699	0.821	0.905	0.998	0.675
NK cell maximum expansion rate	$\rho_K \cdot d_K$	/day	1.951	1.729	1.731	1.485	1.716	1.999	1.467	1.985	1.717	1.977
$CD8^+$ T cell killing stimulation factor	γ_E		7.573	1.283	11.871	27.233	12.747	58.212	0.483	44.171	12.117	39.819
NK cell killing stimulation factor	γ_K		43.206	2.379	0.675	13.068	5.266	0.047	77.088	0.933	92.143	0.112
Tolerance effect factor	η		13.515	18.113	25.085	11.266	16.081	10.496	15.706	9.454	15.353	22.479
Proliferation regulation factor	φ		0.042	0.083	0.011	0.059	0.017	0.063	0.191	0.027	0.010	0.068
Killing regulation factor	λ		10.979	2.064	2.126	11.387	7.191	23.746	14.663	15.609	6.225	22.824

a. Parameters that are marked with **(x 10^3)** display actual parameter values x 10^3. For example, the displayed value of tolerance recovery (τ) for parameter set #1 is 8.289, but the actual value is 0.008289.

Table S7. Fitted parameters for full model (11-20 lowest NLL)

Parameter [a]		Units	#11	#12	#13	#14	#15	#16	#17	#18	#19	#20
N-803 50% effect concentration	C_{50}	pM	3.198	4.655	6.290	2.145	4.141	1.544	1.581	1.161	3.117	3.625
Tolerance rate constant	δ_{TOL}	/day	0.733	0.599	0.705	0.882	0.648	0.410	0.625	0.503	0.516	0.598
Regulation rate constant	δ_{REG}	/day	0.281	4.263	0.158	0.381	0.325	0.177	4.672	3.590	1.627	0.705
Tolerance recovery **(x 10^3)**	τ		3.631	6.056	5.128	3.607	3.029	12.760	4.378	8.182	5.919	5.613
Escape variant initial frequency **(x 10^3)**	f		1.475	41.841	900.056	1.608	1.074	167.981	8.148	211.169	151.142	1.860
Escape variant susceptibility factor **(x 10^3)**	χ		30.481	208.448	968.785	63.724	5.151	87.120	4.491	75.289	743.567	4.469
$CD8^+$ T cell death rate constant	d_E	/day	0.190	0.148	0.114	0.087	0.065	0.062	0.232	0.076	0.186	0.207
NK cell death rate constant	d_K	/day	0.766	0.283	0.491	0.223	0.229	0.670	0.697	0.280	0.374	0.428
$CD8^+$ T cell killing rate constant **(x 10^3)**	g_E	µL/#·d	0.221	0.334	0.057	0.257	0.074	0.066	0.113	0.760	0.239	0.092
NK cell / $CD8^+$ T cell killing rate ratio	g_K/g_E		0.981	0.244	0.533	0.440	0.359	0.199	0.809	0.548	0.095	0.982
Maximum proliferating cells	h	#/µL	1835.705	185.836	711.605	284.254	359.938	763.196	1485.771	34.945	128.414	628.757
$CD8^+$ T cell maximum expansion rate	$\rho_E \cdot d_E$	/day	0.597	1.255	0.853	1.111	0.730	0.339	0.760	0.610	1.104	1.070
NK cell maximum expansion rate	$\rho_K \cdot d_K$	/day	1.398	1.964	1.985	1.992	1.576	1.631	1.515	1.958	1.986	1.546
$CD8^+$ T cell killing stimulation factor	γ_E		0.743	11.208	0.368	0.052	0.498	5.282	0.019	4.231	13.100	0.617
NK cell killing stimulation factor	γ_K		1.429	0.151	29.597	11.314	59.087	55.590	48.485	1.028	0.345	29.054
Tolerance effect factor	η		15.451	13.689	16.487	18.507	18.349	15.601	12.231	9.584	7.805	14.579
Proliferation regulation factor	φ		0.043	0.014	0.056	0.132	0.241	0.048	0.088	0.019	0.014	0.030
Killing regulation factor	λ		2.254	5.954	8.085	2.808	6.637	12.775	6.738	2.521	8.568	6.710

a. Parameters that are marked with **(x 10^3)** display actual parameter values x 10^3. For example, the displayed value of tolerance recovery (τ) for parameter set #1 is 8.289, but the actual value is 0.008289.

Table S8. Fitted parameters for model #1 (1-10 lowest NLL)

Parameter [a]		Units	#1	#2	#3	#4	#5	#6	#7	#8	#9	#10
N-803 50% effect concentration	C_{50}	pM	1.271	1.350	1.172	1.302	1.225	1.034	1.232	1.287	1.125	1.059
Tolerance rate constant	δ_{TOL}	/day	-	-	-	-	-	-	-	-	-	-
Regulation rate constant	δ_{REG}	/day	0.385	0.449	0.368	0.397	0.353	0.425	0.370	0.370	0.397	0.518
Tolerance recovery **(x 10^3)**	τ		-	-	-	-	-	-	-	-	-	-
Escape variant initial frequency **(x 10^3)**	f		115.194	86.190	102.174	69.823	120.150	144.729	75.826	101.846	132.214	115.658
Escape variant susceptibility factor **(x 10^3)**	χ		5.902	4.324	4.562	19.675	2.082	1.136	33.692	36.046	8.439	62.561
$CD8^+$ T cell death rate constant	d_E	/day	0.094	0.086	0.123	0.092	0.079	0.113	0.109	0.076	0.139	0.138
NK cell death rate constant	d_K	/day	0.274	0.245	0.313	0.277	0.273	0.301	0.286	0.248	0.336	0.323
$CD8^+$ T cell killing rate constant **(x 10^3)**	g_E	μL/#·d	1.093	0.514	0.507	0.954	0.237	1.156	0.696	1.298	0.255	1.069
NK cell / $CD8^+$ T cell killing rate ratio	g_K/g_E		0.235	0.390	0.484	0.130	0.942	0.190	0.249	0.144	0.850	0.158
Maximum proliferating cells	h	#/μL	196.073	322.934	199.876	321.970	167.906	259.434	162.866	134.371	274.141	558.197
$CD8^+$ T cell maximum expansion rate	$\rho_E \cdot d_E$	/day	0.831	0.895	0.897	0.724	0.691	0.937	0.884	0.745	0.963	1.010
NK cell maximum expansion rate	$\rho_K \cdot d_K$	/day	1.947	1.980	1.864	1.669	1.898	1.997	1.915	1.954	1.872	1.822
$CD8^+$ T cell killing stimulation factor	γ_E		0.432	1.654	1.110	0.961	4.628	1.695	1.033	0.716	4.458	1.098
NK cell killing stimulation factor	γ_K		0.055	0.013	0.016	0.036	0.127	0.836	0.019	0.146	1.066	0.337
Tolerance effect factor	η		-	-	-	-	-	-	-	-	-	-
Proliferation regulation factor	φ		4.659	6.043	3.783	4.372	4.483	4.547	4.156	4.920	3.740	4.454
Killing regulation factor	λ		2.058	2.347	2.103	3.481	2.285	4.091	3.180	2.968	5.306	3.627

a. Parameters that are marked with **(x 10^3)** display actual parameter values x 10^3. For example, the displayed value of tolerance recovery (τ) for parameter set #1 is 8.289, but the actual value is 0.008289.

Table S9. Fitted parameters for model #1 (11-20 lowest NLL)

Parameter [a]		Units	#11	#12	#13	#14	#15	#16	#17	#18	#19	#20
N-803 50% effect concentration	C_{50}	pM	1.153	2.600	1.588	1.092	1.457	1.344	1.169	1.395	1.215	1.043
Tolerance rate constant	δ_{TOL}	/day	-	-	-	-	-	-	-	-	-	-
Regulation rate constant	δ_{REG}	/day	0.362	0.394	0.488	0.337	0.353	0.334	0.350	0.357	0.382	0.358
Tolerance recovery **(x 10^3)**	τ		-	-	-	-	-	-	-	-	-	-
Escape variant initial frequency **(x 10^3)**	f		88.637	126.971	100.235	110.373	103.419	89.227	84.242	134.012	120.470	136.255
Escape variant susceptibility factor **(x 10^3)**	χ		12.565	1.592	6.680	3.760	18.673	1.984	4.370	28.805	4.001	2.865
$CD8^+$ T cell death rate constant	d_E	/day	0.114	0.091	0.130	0.089	0.075	0.113	0.079	0.079	0.130	0.081
NK cell death rate constant	d_K	/day	0.281	0.293	0.310	0.262	0.265	0.323	0.257	0.243	0.325	0.299
$CD8^+$ T cell killing rate constant **(x 10^3)**	g_E	μL/#·d	0.317	0.595	0.198	0.388	0.510	0.477	0.432	0.255	0.468	1.125
NK cell / $CD8^+$ T cell killing rate ratio	g_K/g_E		0.712	0.418	0.911	0.699	0.477	0.443	0.487	0.785	0.541	0.184
Maximum proliferating cells	h	#/μL	128.841	290.493	514.013	93.610	155.036	147.240	179.746	152.850	298.330	229.024
$CD8^+$ T cell maximum expansion rate	$\rho_E \cdot d_E$	/day	0.934	0.749	1.047	0.767	0.663	0.800	0.683	0.796	0.890	0.659
NK cell maximum expansion rate	$\rho_K \cdot d_K$	/day	1.936	1.914	1.953	1.900	1.883	1.918	1.747	1.939	1.742	1.923
$CD8^+$ T cell killing stimulation factor	γ_E		2.529	1.554	4.702	1.727	1.801	1.669	1.848	4.595	1.140	1.266
NK cell killing stimulation factor	γ_K		0.139	0.069	0.060	0.032	0.152	0.446	0.019	0.893	0.033	0.328
Tolerance effect factor	η		-	-	-	-	-	-	-	-	-	-
Proliferation regulation factor	φ		4.102	4.420	4.942	4.236	4.478	3.510	4.503	5.231	3.734	4.411
Killing regulation factor	λ		2.965	2.281	2.495	2.009	2.885	4.023	2.367	5.356	1.884	2.797

a. Parameters that are marked with **(x 10^3)** display actual parameter values x 10^3. For example, the displayed value of tolerance recovery (τ) for parameter set #1 is 8.289, but the actual value is 0.008289.

Table S10. Fitted parameters for model #2 (1-10 lowest NLL)

Parameter [a]		Units	#1	#2	#3	#4	#5	#6	#7	#8	#9	#10
N-803 50% effect concentration	C_{50}	pM	1.740	5.574	2.952	1.069	2.472	1.056	3.510	5.156	3.841	5.779
Tolerance rate constant	δ_{TOL}	/day	0.523	0.468	0.504	0.404	0.800	0.529	0.477	0.518	0.762	0.635
Regulation rate constant	δ_{REG}	/day	-	-	-	-	-	-	-	-	-	-
Tolerance recovery **(x 10^3)**	τ		3.147	4.300	3.605	7.208	2.138	2.909	2.992	6.496	2.355	6.141
Escape variant initial frequency **(x 10^3)**	f		136.925	172.794	177.554	182.003	141.929	187.318	176.452	242.575	147.496	145.203
Escape variant susceptibility factor **(x 10^3)**	χ		2.157	1.104	19.886	1.987	2.072	2.128	1.511	3.572	1.536	2.073
$CD8^+$ T cell death rate constant	d_E	/day	0.067	0.051	0.050	0.072	0.121	0.083	0.066	0.094	0.160	0.118
NK cell death rate constant	d_K	/day	0.337	0.315	0.347	0.682	0.365	0.552	0.457	0.739	0.442	0.321
$CD8^+$ T cell killing rate constant **(x 10^3)**	g_E	μL/#·d	0.030	0.064	0.021	0.054	0.023	0.020	0.643	0.050	0.440	0.093
NK cell / $CD8^+$ T cell killing rate ratio	g_K/g_E		0.040	0.113	0.066	0.087	0.103	0.069	0.017	0.250	0.010	0.031
Maximum proliferating cells	h	#/μL	373.126	423.787	647.820	562.346	699.387	1356.583	928.114	1504.481	868.840	634.284
$CD8^+$ T cell maximum expansion rate	$\rho_E \cdot d_E$	/day	0.636	0.568	0.478	0.399	1.112	0.554	0.545	0.494	1.122	1.020
NK cell maximum expansion rate	$\rho_K \cdot d_K$	/day	1.944	1.832	1.515	1.967	1.990	1.595	1.751	1.794	1.988	1.784
$CD8^+$ T cell killing stimulation factor	γ_E		41.741	21.037	93.275	74.797	79.424	85.032	0.056	97.756	0.120	12.045
NK cell killing stimulation factor	γ_K		0.015	0.470	2.048	2.644	0.961	53.394	1.249	0.050	0.039	0.060
Tolerance effect factor	η		29.527	36.093	30.037	17.914	31.021	49.926	48.498	28.273	26.590	31.141
Proliferation regulation factor	φ		-	-	-	-	-	-	-	-	-	-
Killing regulation factor	λ		-	-	-	-	-	-	-	-	-	-

a. Parameters that are marked with **(x 10^3)** display actual parameter values x 10^3. For example, the displayed value of tolerance recovery (τ) for parameter set #1 is 8.289, but the actual value is 0.008289.

Table S11. Fitted parameters for model #2 (11-20 lowest NLL)

Parameter [a]		Units	#11	#12	#13	#14	#15	#16	#17	#18	#19	#20
N-803 50% effect concentration	C_{50}	pM	1.653	2.846	1.703	6.598	1.899	3.081	2.108	1.133	1.372	6.249
Tolerance rate constant	δ_{TOL}	/day	0.508	0.676	0.476	0.466	0.554	0.768	0.573	0.415	0.446	0.511
Regulation rate constant	δ_{REG}	/day	-	-	-	-	-	-	-	-	-	-
Tolerance recovery **(x 10^3)**	τ		6.971	3.640	12.190	9.067	2.016	3.718	1.240	15.340	9.705	4.178
Escape variant initial frequency **(x 10^3)**	f		193.884	204.756	163.434	195.250	443.382	188.320	154.947	196.346	151.737	191.460
Escape variant susceptibility factor **(x 10^3)**	χ		2.866	3.298	1.088	1.993	1.196	5.911	7.317	9.732	1.621	3.152
$CD8^+$ T cell death rate constant	d_E	/day	0.103	0.095	0.083	0.137	0.050	0.115	0.064	0.058	0.076	0.050
NK cell death rate constant	d_K	/day	0.438	0.313	0.483	0.998	0.377	0.391	0.491	0.646	0.500	0.245
$CD8^+$ T cell killing rate constant **(x 10^3)**	g_E	μL/#·d	0.110	0.340	0.997	0.020	0.195	0.066	0.021	0.027	0.173	0.146
NK cell / $CD8^+$ T cell killing rate ratio	g_K/g_E		0.043	0.027	0.015	0.031	0.014	0.063	0.010	0.061	0.021	0.011
Maximum proliferating cells	h	#/μL	354.408	498.465	491.897	1819.032	554.522	625.954	1451.328	797.919	807.452	140.772
$CD8^+$ T cell maximum expansion rate	$\rho_E \cdot d_E$	/day	0.716	0.973	0.539	0.536	0.590	0.982	0.634	0.331	0.342	0.644
NK cell maximum expansion rate	$\rho_K \cdot d_K$	/day	2.000	1.967	1.799	1.997	1.998	1.934	1.992	1.505	1.061	1.992
$CD8^+$ T cell killing stimulation factor	γ_E		10.492	11.910	0.010	99.193	2.264	27.761	96.123	95.236	4.146	96.779
NK cell killing stimulation factor	γ_K		0.075	0.020	0.010	99.683	91.831	9.787	0.025	1.028	1.619	0.200
Tolerance effect factor	η		16.143	31.461	18.868	28.459	37.951	22.168	93.652	19.655	14.355	23.531
Proliferation regulation factor	φ		-	-	-	-	-	-	-	-	-	-
Killing regulation factor	λ		-	-	-	-	-	-	-	-	-	-

a. Parameters that are marked with **(x 10^3)** display actual parameter values x 10^3. For example, the displayed value of tolerance recovery (τ) for parameter set #1 is 8.289, but the actual value is 0.008289.

Table S12. Fitted parameters for model #3 (1-10 lowest NLL)

Parameter [a]		Units	#1	#2	#3	#4	#5	#6	#7	#8	#9	#10
N-803 50% effect concentration	C_{50}	pM	2.220	1.066	2.933	1.167	2.383	1.390	1.860	5.801	3.746	1.015
Tolerance rate constant	δ_{TOL}	/day	1.040	0.500	1.029	0.497	0.949	0.503	1.040	0.793	0.448	1.485
Regulation rate constant	δ_{REG}	/day	0.350	4.199	0.560	4.711	0.204	1.169	0.173	0.296	0.843	0.335
Tolerance recovery **(x 10^3)**	τ		2.221	7.833	3.511	7.900	5.070	8.130	2.165	4.432	11.165	2.098
Escape variant initial frequency **(x 10^3)**	f		-	-	-	-	-	-	-	-	-	-
Escape variant susceptibility factor **(x 10^3)**	χ		-	-	-	-	-	-	-	-	-	-
$CD8^+$ T cell death rate constant	d_E	/day	0.184	0.083	0.177	0.139	0.095	0.089	0.137	0.120	0.065	0.227
NK cell death rate constant	d_K	/day	0.476	0.522	0.458	0.432	0.332	0.459	0.563	0.399	0.373	0.422
$CD8^+$ T cell killing rate constant **(x 10^3)**	g_E	µL/#·d	0.178	0.095	0.091	0.158	0.107	0.104	0.187	0.147	0.114	0.344
NK cell / $CD8^+$ T cell killing rate ratio	g_K/g_E		0.287	0.881	0.104	0.855	0.182	0.013	0.026	0.804	0.015	0.011
Maximum proliferating cells	h	#/µL	1985.398	535.917	1988.361	164.684	975.801	450.613	1970.102	1159.726	274.799	1973.867
$CD8^+$ T cell maximum expansion rate	$\rho_E \cdot d_E$	/day	0.938	0.499	1.070	0.753	0.885	0.584	0.948	0.980	0.516	1.437
NK cell maximum expansion rate	$\rho_K \cdot d_K$	/day	1.512	1.828	1.684	1.989	1.732	1.911	1.887	1.981	1.962	1.752
$CD8^+$ T cell killing stimulation factor	γ_E		6.408	0.024	46.763	0.086	9.556	84.542	4.060	0.033	62.203	0.619
NK cell killing stimulation factor	γ_K		0.039	77.469	1.504	31.018	1.878	2.017	0.011	7.952	30.503	25.697
Tolerance effect factor	η		16.447	16.530	18.733	8.229	22.784	17.209	30.891	35.998	15.717	18.929
Proliferation regulation factor	φ		0.178	0.011	0.194	0.011	0.161	0.017	0.091	0.047	0.026	0.181
Killing regulation factor	λ		4.074	10.575	24.792	6.159	4.695	32.878	3.000	3.226	32.545	1.719

a. Parameters that are marked with **(x 10^3)** display actual parameter values x 10^3. For example, the displayed value of tolerance recovery (τ) for parameter set #1 is 8.289, but the actual value is 0.008289.

Table S13. Fitted parameters for model #3 (11-20 lowest NLL)

Parameter [a]		Units	#11	#12	#13	#14	#15	#16	#17	#18	#19	#20
N-803 50% effect concentration	C_{50}	pM	1.100	3.449	3.084	2.403	1.134	3.183	1.297	1.274	1.037	3.636
Tolerance rate constant	δ_{TOL}	/day	0.604	0.577	0.518	0.717	0.759	0.748	0.518	1.450	0.594	0.701
Regulation rate constant	δ_{REG}	/day	3.286	4.610	1.390	0.163	4.508	0.182	2.726	0.384	4.695	1.098
Tolerance recovery **(x 10^3)**	τ		5.905	5.092	6.076	5.356	3.393	4.357	6.117	2.564	3.700	5.583
Escape variant initial frequency **(x 10^3)**	f		-	-	-	-	-	-	-	-	-	-
Escape variant susceptibility factor **(x 10^3)**	χ		-	-	-	-	-	-	-	-	-	-
$CD8^+$ T cell death rate constant	d_E	/day	0.154	0.231	0.143	0.092	0.189	0.069	0.111	0.183	0.125	0.136
NK cell death rate constant	d_K	/day	0.276	0.565	0.295	0.292	0.328	0.236	0.290	0.379	0.220	0.289
$CD8^+$ T cell killing rate constant **(x 10^3)**	g_E	μL/#·d	0.313	0.148	0.132	0.156	0.172	0.029	0.196	0.216	0.135	0.133
NK cell / $CD8^+$ T cell killing rate ratio	g_K/g_E		0.269	0.625	0.133	0.011	0.885	0.011	0.051	0.940	0.959	0.016
Maximum proliferating cells	h	#/μL	27.445	700.899	150.454	447.663	355.404	252.872	87.694	1772.321	21.111	382.441
$CD8^+$ T cell maximum expansion rate	$\rho_E \cdot d_E$	/day	1.105	1.013	0.993	0.873	1.516	0.854	0.723	1.682	1.106	1.261
NK cell maximum expansion rate	$\rho_K \cdot d_K$	/day	1.962	1.768	1.795	1.883	1.983	1.972	1.643	1.990	1.946	1.999
$CD8^+$ T cell killing stimulation factor	γ_E		0.049	0.020	43.916	4.353	9.906	76.314	40.684	0.337	55.073	24.526
NK cell killing stimulation factor	γ_K		41.747	73.073	5.718	26.397	18.662	0.468	0.551	0.243	0.011	99.517
Tolerance effect factor	η		7.663	11.701	11.196	21.515	11.738	17.201	8.595	23.483	11.123	20.681
Proliferation regulation factor	φ		0.019	0.071	0.027	0.037	0.146	0.195	0.024	0.202	0.019	0.023
Killing regulation factor	λ		3.789	9.276	20.722	3.750	5.822	66.789	18.828	1.840	14.911	10.214

a. Parameters that are marked with **(x 10^3)** display actual parameter values x 10^3. For example, the displayed value of tolerance recovery (τ) for parameter set #1 is 8.289, but the actual value is 0.008289.

Table S14. Fitted parameters for model #4 (1-10 lowest NLL)

Parameter [a]		Units	#1	#2	#3	#4	#5	#6	#7	#8	#9	#10
N-803 50% effect concentration	C_{50}	pM	1.114	1.400	1.556	1.429	1.076	1.307	1.111	1.351	1.218	1.359
Tolerance rate constant	δ_{TOL}	/day	-	-	-	-	-	-	-	-	-	-
Regulation rate constant	δ_{REG}	/day	0.649	0.507	0.631	0.531	0.532	0.513	0.511	0.516	0.586	0.539
Tolerance recovery **(x 10^3)**	τ		-	-	-	-	-	-	-	-	-	-
Escape variant initial frequency **(x 10^3)**	f		-	-	-	-	-	-	-	-	-	-
Escape variant susceptibility factor **(x 10^3)**	χ		-	-	-	-	-	-	-	-	-	-
$CD8^+$ T cell death rate constant	d_E	/day	0.157	0.123	0.147	0.117	0.125	0.133	0.132	0.124	0.145	0.130
NK cell death rate constant	d_K	/day	0.378	0.345	0.313	0.303	0.327	0.348	0.371	0.313	0.334	0.298
$CD8^+$ T cell killing rate constant **(x 10^3)**	g_E	μL/#·d	0.826	0.424	1.179	0.781	0.371	0.529	0.246	0.516	1.164	0.469
NK cell / $CD8^+$ T cell killing rate ratio	g_K/g_E		0.171	0.043	0.167	0.313	0.271	0.025	0.233	0.100	0.016	0.030
Maximum proliferating cells	h	#/μL	965.892	590.877	676.168	560.175	542.932	614.032	633.186	572.691	687.686	609.204
$CD8^+$ T cell maximum expansion rate	$\rho_E \cdot d_E$	/day	1.022	0.900	1.165	0.965	0.983	0.977	0.864	0.965	1.031	1.103
NK cell maximum expansion rate	$\rho_K \cdot d_K$	/day	1.949	1.954	1.928	1.900	1.983	1.964	1.879	1.879	1.845	1.941
$CD8^+$ T cell killing stimulation factor	γ_E		0.027	0.163	0.020	0.167	0.422	0.240	0.687	0.388	0.233	0.284
NK cell killing stimulation factor	γ_K		3.523	49.811	1.111	0.852	8.430	43.605	25.254	10.933	0.598	48.935
Tolerance effect factor	η		-	-	-	-	-	-	-	-	-	-
Proliferation regulation factor	φ		4.403	4.505	4.955	4.967	4.795	4.543	4.046	4.798	4.459	5.338
Killing regulation factor	λ		2.252	4.250	1.953	2.272	4.560	3.321	8.696	3.595	2.208	3.818

a. Parameters that are marked with **(x 10^3)** display actual parameter values x 10^3. For example, the displayed value of tolerance recovery (τ) for parameter set #1 is 8.289, but the actual value is 0.008289.

Table S15. Fitted parameters for model #4 (11-20 lowest NLL)

Parameter [a]		Units	#11	#12	#13	#14	#15	#16	#17	#18	#19	#20
N-803 50% effect concentration	C_{50}	pM	1.606	1.088	1.390	1.052	1.113	2.336	2.847	1.430	2.080	1.132
Tolerance rate constant	δ_{TOL}	/day	-	-	-	-	-	-	-	-	-	-
Regulation rate constant	δ_{REG}	/day	0.510	0.519	0.592	0.640	0.517	0.499	0.452	0.602	0.634	0.532
Tolerance recovery **(x 10^3)**	τ		-	-	-	-	-	-	-	-	-	-
Escape variant initial frequency **(x 10^3)**	f		-	-	-	-	-	-	-	-	-	-
Escape variant susceptibility factor **(x 10^3)**	χ		-	-	-	-	-	-	-	-	-	-
$CD8^+$ T cell death rate constant	d_E	/day	0.106	0.135	0.183	0.183	0.151	0.152	0.109	0.174	0.166	0.125
NK cell death rate constant	d_K	/day	0.245	0.436	0.473	0.431	0.320	0.339	0.251	0.435	0.400	0.336
$CD8^+$ T cell killing rate constant **(x 10^3)**	g_E	μL/#·d	0.874	0.200	0.398	0.383	0.317	0.226	0.356	0.192	0.341	0.102
NK cell / $CD8^+$ T cell killing rate ratio	g_K/g_E		0.383	0.540	0.096	0.072	0.048	0.264	0.042	0.553	0.489	0.748
Maximum proliferating cells	h	#/μL	365.399	846.330	1129.423	1021.995	491.792	607.596	348.871	1108.214	1385.490	819.918
$CD8^+$ T cell maximum expansion rate	$\rho_E \cdot d_E$	/day	1.113	0.735	0.884	1.057	1.146	1.113	1.122	0.902	0.982	0.865
NK cell maximum expansion rate	$\rho_K \cdot d_K$	/day	1.948	1.845	1.819	1.979	1.903	1.946	1.995	1.785	1.897	1.799
$CD8^+$ T cell killing stimulation factor	γ_E		0.072	1.359	0.283	0.626	0.158	0.060	0.344	0.532	0.481	0.031
NK cell killing stimulation factor	γ_K		0.026	13.690	27.964	43.118	68.441	28.275	66.138	22.275	6.235	87.670
Tolerance effect factor	η		-	-	-	-	-	-	-	-	-	-
Proliferation regulation factor	φ		5.910	3.531	3.271	3.903	4.566	4.482	5.841	3.506	4.242	4.620
Killing regulation factor	λ		1.882	10.404	5.042	6.203	5.173	9.396	5.671	13.183	5.430	57.221

a. Parameters that are marked with **(x 10^3)** display actual parameter values x 10^3. For example, the displayed value of tolerance recovery (τ) for parameter set #1 is 8.289, but the actual value is 0.008289.

References

1. Ellis-Connell AL, Balgeman AJ, Zarbock KR, Barry G, Weiler A, Egan JO, et al. ALT-803 Transiently Reduces Simian Immunodeficiency Virus Replication in the Absence of Antiretroviral Treatment. Journal of virology. 2018;92(3). Epub 2017/11/10. doi: 10.1128/jvi.01748-17. PubMed PMID: 29118125; PubMed Central PMCID: PMCPMC5774892.
2. Haase AT. Population biology of HIV-1 infection: viral and CD4+ T cell demographics and dynamics in lymphatic tissues. Annual review of immunology. 1999;17:625-56. Epub 1999/06/08. doi: 10.1146/annurev.immunol.17.1.625. PubMed PMID: 10358770.
3. Ramratnam B, Bonhoeffer S, Binley J, Hurley A, Zhang L, Mittler JE, et al. Rapid production and clearance of HIV-1 and hepatitis C virus assessed by large volume plasma apheresis. Lancet (London, England). 1999;354(9192):1782-5. Epub 1999/11/30. doi: 10.1016/s0140-6736(99)02035-8. PubMed PMID: 10577640.
4. Zhang L, Dailey PJ, He T, Gettie A, Bonhoeffer S, Perelson AS, et al. Rapid clearance of simian immunodeficiency virus particles from plasma of rhesus macaques. Journal of virology. 1999;73(1):855-60. Epub 1998/12/16. PubMed PMID: 9847402; PubMed Central PMCID: PMCPMC103903.
5. Zhang L, Dailey PJ, Gettie A, Blanchard J, Ho DD. The liver is a major organ for clearing simian immunodeficiency virus in rhesus monkeys. Journal of virology. 2002;76(10):5271-3. Epub 2002/04/23. PubMed PMID: 11967341; PubMed Central PMCID: PMCPMC136155.
6. Cardozo EF, Andrade A, Mellors JW, Kuritzkes DR, Perelson AS, Ribeiro RM. Treatment with integrase inhibitor suggests a new interpretation of HIV RNA decay curves that reveals a subset of cells with slow integration. PLoS pathogens. 2017;13(7):e1006478. Epub 2017/07/06. doi: 10.1371/journal.ppat.1006478. PubMed PMID: 28678879; PubMed Central PMCID: PMCPMC5513547.
7. Conway JM, Perelson AS. Residual Viremia in Treated HIV+ Individuals. PLoS computational biology. 2016;12(1):e1004677. Epub 2016/01/07. doi: 10.1371/journal.pcbi.1004677. PubMed PMID: 26735135; PubMed Central PMCID: PMCPMC4703306.
8. Zimmermann C, Prévost-Blondel A, Blaser C, Pircher H. Kinetics of the response of naive and memory CD8 T cells to antigen: similarities and differences. European journal of immunology. 1999;29(1):284-90. Epub 1999/02/05. doi: 10.1002/(sici)1521-4141(199901)29:01<284::Aid-immu284>3.0.Co;2-c. PubMed PMID: 9933110.

9. Veiga-Fernandes H, Walter U, Bourgeois C, McLean A, Rocha B. Response of naïve and memory CD8+ T cells to antigen stimulation in vivo. Nature immunology. 2000;1(1):47-53. Epub 2001/03/23. doi: 10.1038/76907. PubMed PMID: 10881174.

10. Kim TS, Shin EC. The activation of bystander CD8(+) T cells and their roles in viral infection. Experimental & molecular medicine. 2019;51(12):1-9. Epub 2019/12/13. doi: 10.1038/s12276-019-0316-1. PubMed PMID: 31827070; PubMed Central PMCID: PMCPMC6906361.

11. Younes SA, Freeman ML, Mudd JC, Shive CL, Reynaldi A, Panigrahi S, et al. IL-15 promotes activation and expansion of CD8+ T cells in HIV-1 infection. The Journal of clinical investigation. 2016;126(7):2745-56. Epub 2016/06/21. doi: 10.1172/jci85996. PubMed PMID: 27322062; PubMed Central PMCID: PMCPMC4922693.

12. Bastidas S, Graw F, Smith MZ, Kuster H, Günthard HF, Oxenius A. CD8+ T cells are activated in an antigen-independent manner in HIV-infected individuals. Journal of immunology (Baltimore, Md : 1950). 2014;192(4):1732-44. Epub 2014/01/22. doi: 10.4049/jimmunol.1302027. PubMed PMID: 24446519.

13. Kim J, Chang DY, Lee HW, Lee H, Kim JH, Sung PS, et al. Innate-like Cytotoxic Function of Bystander-Activated CD8(+) T Cells Is Associated with Liver Injury in Acute Hepatitis A. Immunity. 2018;48(1):161-73.e5. Epub 2018/01/07. doi: 10.1016/j.immuni.2017.11.025. PubMed PMID: 29305140.

14. Lin JX, Leonard WJ. The Common Cytokine Receptor γ Chain Family of Cytokines. Cold Spring Harbor perspectives in biology. 2018;10(9). Epub 2017/10/19. doi: 10.1101/cshperspect.a028449. PubMed PMID: 29038115; PubMed Central PMCID: PMCPMC6120701.

15. Au-Yeung BB, Smith GA, Mueller JL, Heyn CS, Jaszczak RG, Weiss A, et al. IL-2 Modulates the TCR Signaling Threshold for CD8 but Not CD4 T Cell Proliferation on a Single-Cell Level. Journal of immunology (Baltimore, Md : 1950). 2017;198(6):2445-56. Epub 2017/02/06. doi: 10.4049/jimmunol.1601453. PubMed PMID: 28159902; PubMed Central PMCID: PMCPMC5340617.

16. Malek TR. The biology of interleukin-2. Annual review of immunology. 2008;26:453-79. Epub 2007/12/08. doi: 10.1146/annurev.immunol.26.021607.090357. PubMed PMID: 18062768.

17. Papillion A, Powell MD, Chisolm DA, Bachus H, Fuller MJ, Weinmann AS, et al. Inhibition of IL-2 responsiveness by IL-6 is required for the generation of GC-TFH cells. Science

immunology. 2019;4(39). Epub 2019/09/15. doi: 10.1126/sciimmunol.aaw7636. PubMed PMID: 31519812; PubMed Central PMCID: PMCPMC6820141.

18. Lugli E, Goldman CK, Perera LP, Smedley J, Pung R, Yovandich JL, et al. Transient and persistent effects of IL-15 on lymphocyte homeostasis in nonhuman primates. Blood. 2010;116(17):3238-48. Epub 2010/07/16. doi: 10.1182/blood-2010-03-275438. PubMed PMID: 20631381; PubMed Central PMCID: PMCPMC2995354.

19. McKay MD, Beckman RJ, Conover WJ. Comparison of Three Methods for Selecting Values of Input Variables in the Analysis of Output from a Computer Code. Technometrics. 1979;21(2):239-45. doi: 10.1080/00401706.1979.10489755.

20. Byrd RH, Gilbert JC, Nocedal J. A trust region method based on interior point techniques for nonlinear programming. Mathematical Programming. 2000;89(1):149-85. doi: 10.1007/PL00011391.

21. Rhode PR, Egan JO, Xu W, Hong H, Webb GM, Chen X, et al. Comparison of the Superagonist Complex, ALT-803, to IL15 as Cancer Immunotherapeutics in Animal Models. Cancer immunology research. 2016;4(1):49-60. Epub 2015/10/30. doi: 10.1158/2326-6066.cir-15-0093-t. PubMed PMID: 26511282; PubMed Central PMCID: PMCPMC4703482.

22. Romee R, Cooley S, Berrien-Elliott MM, Westervelt P, Verneris MR, Wagner JE, et al. First-in-human phase 1 clinical study of the IL-15 superagonist complex ALT-803 to treat relapse after transplantation. Blood. 2018;131(23):2515-27. Epub 2018/02/22. doi: 10.1182/blood-2017-12-823757. PubMed PMID: 29463563; PubMed Central PMCID: PMCPMC5992862.

23. Han KP, Zhu X, Liu B, Jeng E, Kong L, Yovandich JL, et al. IL-15:IL-15 receptor alpha superagonist complex: high-level co-expression in recombinant mammalian cells, purification and characterization. Cytokine. 2011;56(3):804-10. Epub 2011/10/25. doi: 10.1016/j.cyto.2011.09.028. PubMed PMID: 22019703; PubMed Central PMCID: PMCPMC3221918.

24. Webb GM, Li S, Mwakalundwa G, Folkvord JM, Greene JM, Reed JS, et al. The human IL-15 superagonist ALT-803 directs SIV-specific CD8(+) T cells into B-cell follicles. Blood advances. 2018;2(2):76-84. Epub 2018/01/25. doi: 10.1182/bloodadvances.2017012971. PubMed PMID: 29365313; PubMed Central PMCID: PMCPMC5787870.

25. Gadhamsetty S, Beltman JB, de Boer RJ. What do mathematical models tell us about killing rates during HIV-1 infection? Immunology letters. 2015;168(1):1-6. Epub 2015/08/19. doi: 10.1016/j.imlet.2015.07.009. PubMed PMID: 26279491.

26. Jin X, Bauer DE, Tuttleton SE, Lewin S, Gettie A, Blanchard J, et al. Dramatic rise in plasma viremia after CD8(+) T cell depletion in simian immunodeficiency virus-infected macaques. The Journal of experimental medicine. 1999;189(6):991-8. Epub 1999/03/17. doi: 10.1084/jem.189.6.991. PubMed PMID: 10075982; PubMed Central PMCID: PMCPMC2193038.

27. Choi EI, Reimann KA, Letvin NL. In vivo natural killer cell depletion during primary simian immunodeficiency virus infection in rhesus monkeys. Journal of virology. 2008;82(13):6758-61. Epub 2008/04/25. doi: 10.1128/jvi.02277-07. PubMed PMID: 18434394; PubMed Central PMCID: PMCPMC2447079.

28. De Boer RJ, Mohri H, Ho DD, Perelson AS. Turnover rates of B cells, T cells, and NK cells in simian immunodeficiency virus-infected and uninfected rhesus macaques. Journal of immunology (Baltimore, Md : 1950). 2003;170(5):2479-87. Epub 2003/02/21. doi: 10.4049/jimmunol.170.5.2479. PubMed PMID: 12594273.

29. Davenport MP, Ribeiro RM, Perelson AS. Kinetics of virus-specific CD8+ T cells and the control of human immunodeficiency virus infection. Journal of virology. 2004;78(18):10096-103. Epub 2004/08/28. doi: 10.1128/jvi.78.18.10096-10103.2004. PubMed PMID: 15331742; PubMed Central PMCID: PMCPMC515020.

30. Akaike H. A new look at the statistical model identification. IEEE Trans Automat Contr. 1974;19(6):716-23.

31. Marino S, Hogue IB, Ray CJ, Kirschner DE. A methodology for performing global uncertainty and sensitivity analysis in systems biology. Journal of theoretical biology. 2008;254(1):178-96. Epub 2008/06/24. doi: 10.1016/j.jtbi.2008.04.011. PubMed PMID: 18572196; PubMed Central PMCID: PMCPMC2570191.